Consumption of atmospheric methane by the Qinghai–Tibetan Plateau alpine steppe ecosystem

Hanbo Yun[1, 2, 3], Qingbai Wu[1*], Qianlai Zhuang[3*], Anping Chen[4*] Tong Yu[3], Zhou Lyu[3], Yuzhong Yang[1], Huijun Jin[1], Guojun Liu[1], Yang Qu[3], Licheng Liu[3]

1. State Key Laboratory of Frozen Soil Engineering, Northwest Institute of Eco–Environment and Resources, Chinese Academy of Sciences, Lanzhou, Gansu 730000, China

2. Key Laboratory for Land Surface Process and Climate Change in Cold and Arid Regions, Chinese Academy of Sciences, Lanzhou, 730000, China

3. Department of Earth, Atmospheric, and Planetary Sciences, Purdue University, West Lafayette, Indiana 47907, USA

4. Department of Forestry and Natural Resources, Purdue University, West Lafayette, Indiana 47907, USA

***Authors for correspondence: qbwu@lzb.ac.cn [Q. W.]，qzhuang@purdue.edu[Q.Z], apchen1111@gmail.com [A.C.]**

A manuscript for *The Cryosphere*

May 30, 2018

Abstract

The Methane (CH_4) cycle on the Qinghai–Tibetan Plateau (QTP), the world's largest high–elevation permafrost region, is sensitive to climate change and subsequent freezing and thawing dynamics. Yet, its magnitudes, patterns, and environmental controls are still poorly understood. Here, we report results from five continuous year–round CH_4 observations from a typical alpine steppe ecosystem in the QTP permafrost region. Our results suggest that the QTP permafrost region was a CH_4 sink of -0.86 ± 0.23 g CH_4–C m^{-2} yr^{-1} over 2012 – 2016, a rate higher than that of many other permafrost areas, such as the Arctic tundra in northern Greenland, Alaska, and western Siberia. Soil temperature and soil water content were dominant factors controlling CH_4 fluxes, however, their correlations changed with soil depths, due to freezing and thawing dynamics. This region was a net CH_4 sink in autumn, but a net source in spring, despite both seasons experiencing similar top soil thawing and freezing dynamics. The opposite CH_4 source/sink function in spring versus in autumn was likely caused by the respective seasons specialized freezing and thawing processes, which modified the vertical distribution of soil layers that are highly mixed in autumn, but not in spring. Furthermore, the traditional definition of four seasons failed to capture the pattern of the annual CH_4 cycle. We developed a new seasonal division method based on soil temperature, bacterial activity, and permafrost active layer thickness, which significantly improved the modelling of the annual CH_4 cycle. Collectively, our findings highlight the critical role of fine–scale climate freezing and thawing dynamics in driving permafrost CH_4 dynamics, which needs to be better monitored and modelled in Earth system models.

1. Introduction

Since 2007, the global atmospheric methane concentration [CH_4] continues to rise, after remaining stable between the 1990s and 2006 (Rigby et al., 2008; IPCC, 2013; Patra and Kort, 2016). Understanding mechanisms for this recent increase requires improved knowledge on methane (CH_4) sources and sinks for regional and global CH_4 budgets (Kirschke et al., 2013; Zona et al., 2016). However, estimates on global CH_4 emissions and consumptions are still highly uncertain (Spahni et al., 2011; Kirschke, 2013). In particular, the bottom–up approach, which estimates CH_4 budgets using ground observations and inventory, overestimated the global CH_4 budget by 6～20 times, compared to the atmospherically constrained top–down approach (Zhu et al., 2004; Lau et al., 2015). This discrepancy is partly due to limited monitoring data and to our poor understanding of important factors regulating the production and consumption of CH_4 (Whalen and Reeburgh, 1990; Dengel et al., 2013; Bohn et al., 2015).

The Qinghai–Tibetan Plateau (QTP) is the world's largest high–elevation permafrost region of 1.23×10^6 km^{-2} (Wang et al., 2000). The QTP is currently experiencing a rapid change in climate, which affects freezing and thawing processes. The change in the freezing and thawing dynamic profoundly impacts methanotrophy and methanogenesis, which consequently impacts net CH_4 fluxes (Mastepanov *et al*., 2013; Lau et al., 2015). However, due to the scarcity of high temporal–resolution year–round environment and CH_4 monitoring, we still know little about the size, seasonal pattern, and underlying controls of climate and permafrost freezing and thawing, and the resulting effects on CH_4 exchanges in the QTP permafrost region (Cao et al., 2008; Wei et al., 2015a; Song et al., 2015;). This knowledge gap also hampers our capacity to predict and understand QTP permafrost CH_4 cycles under current and projected future climates.

Here, we report results from a 5–year continuous *in situ* monitoring of CH_4 dynamics with an eddy covariance (EC) technique at the Beilu'he Research Station, which is a representative site for QTP permafrost heartland. The site was covered by alpine steppe vegetation from January 1st, 2012 to December 31st, 2016. The primary aims of this investigation are to understand (1) the long-term annual and seasonal variation of the methane budget for a typical alpine permafrost site in the QTP, and (2) the environmental factors controlling these CH4 variations and possible underlying mechanisms. In addition, while the consumption and production of ecosystem methane are known through microbial activities, conventional investigations on seasonal methane fluxes usually used climate or vegetation defined "seasons". Therefore, a third research goal of this current study is to investigate if the classical vegetation productivity-based definition of growing season will be useful for defining the methane flux seasonality.

There are three advantages of our data acquisition system. First, the EC system recorded the data of CH_4 fluxes, climate, and soil properties every half hour. As the QTP permafrost is characterized by a rapidly changing climate and a rapidly changing soil freezing and thawing dynamic, even over a time period as short as one day, different aerobic or anaerobic soil environments that favor different types of CH_4 bacteria may change (Rivkina et al., 2004; Lau et al., 2015). Thus, high–resolution *in situ* monitoring data enables us to quantify CH_4 exchange patterns from diel to annual time–scales and investigate their major environmental drivers. Second, our field investigation spanned five full calendar years, including both plant growing and non–growing seasons. Observations of the plant non–growing season, which accounts for two-thirds of a year, were very rare in current literature (Song et al., 2015). Third, the EC system we used overcame some technical problems caused by the often used static chambers, including

limited representation of local site heterogeneity and additional heating of the soil surface (Chang et al., 2014; Wei et al., 2015b).

2. Methods

2.1 Site Description

The research site, Beilu'he permafrost research station (34° 09' 006" N, 92° 02' 080" E), is located in the alpine steppe continuous permafrost area of the northern QTP, about 320 kilometers southwest of Golmud, Qinghai Province (Figure 1). At an elevation of 4765 meters, the air is thin with only 0.6 standard atmospheric pressure. According to *in situ* observations, the site receives solar radiation of about 6720 MJ meter^{-2}. The non–growing season is long and cold, with 225 days per year having an annual air temperature of -18 ℃ on average from 2012 to 2016. The site's growing season is short and cool, with 140 days per year from 2012 to 2016, and a mean annual air temperature of 4.6 °C. According to the site drilling exploration, the permafrost depth can extend to 50 − 70 m belowground, and the thickness of the active layer (ALT) is about 2.2 − 4.8 m. The soil is composed of Quaternary fine sand or silt (Table 1), overlying on Triassic mudstone or weathered marl. Dominant plant species include: *Carex moorcroftii Falc. ex Boott*, *Kobresia tibetica Maxim*, *Androsace tanggulashanensis*, and *Rhodiola tibetica.* Vegetation coverage is approximately 33.5% and the average plant height is 15 cm.

2.2 Eddy Covariance observations

We have continuously monitored CH_4, carbon dioxide (CO_2), water (H_2O), and heat flux using a standard eddy covariance system tower 3 meters above the ground. CH_4 flux was measured with an open-path CH_4 analyzer system (Figure 1: d; LI–7700, LI–COR Inc., Lincoln, NE, USA).

The precision is 5 ppb, with RMS noise at 10 Hz and 2000 ppb. The instrument was placed on site on August 8th, 2011, and then connected to a three–dimensional sonic anemometer (heat and water flux; CSAT3, Campbell Scientific, and Logan, UT, USA; precision is 0.1 °C; accuracy is within 1% of reading for half–hour) and an open–path infrared gas analyzer (CO_2 flux; LI–7500A, LI–COR Inc., Lincoln, NE, USA; the precision is 0.01μmol m^{-2} s^{-1} and the accuracy is within 1% of reading for half–hour, zero drift per °C is ± 0.1 ppm typical) on January 1st, 2012, when the system worked steadily. Monitoring data was recorded and stored at 10 Hz using a data logger (LI–7550, LI–COR Inc., Lincoln, NE, USA).

The operation, calibrations, and maintenance of the EC system followed standard procedures. To reduce the LI–7500A surface heating/cooling influence on CO_2 and H_2O molar densities in tough environments, each year "summer style" was used in Li–7500A, in which surface temperature setting is 5 °C during May 1st to September 30th. "Winter style" was used from October 1st to the next year April 30th in Li–7500A, in which surface temperature setting is -5 °C. Calibrations of CO_2, water vapor, and dew point generator measurements for LI–7500A analyzers were performed regularly by the China Land–Atmosphere Coordinated Observation System (CLAROS). Up–and–down mirrors of LI–COR 7700 were cleaned regularly every 30 days to make sure the signal strength was stronger than 80. All of these instruments were powered by solar–panel and battery.

2.3 Micrometeorological and Soil Measurements

A wide range of meteorological variables were measured by a standard automatic meteorological tower 3 meters above the ground and 5 meters north of the eddy covariance tower. Net radiation (Rn) and albedo were measured with a four–component radiometer (Rn; CNR–1, Kipp and Zonen, the Netherlands). Air temperature (T_{air}), air relative humidity, and

atmospheric pressure were measured with a temperature and humidity sensor (HMP45C, Vaisala Inc., Helsinki, Finland) in the meteorological tower. A rain gauge (TE525MM, Texas Electronics Inc., Dallas, TX, USA) was used to measure the precipitation process. Wind speed and wind direction were observed using a propeller anemometer placed on the top of the meteorological tower.

We also measured soil heat fluxes, soil temperature and soil relative water content (SWC). In August 2010, we installed soil environmental sensors 10 meters from the eddy covariance tower for soil sample collection. Two self–calibrating soil heat flux (SHF) sensors (HFP01) were placed 5 cm and 15 cm below the ground. A group pF–Meter sensor (GEO–Precision, Germany) was embedded in the soil under the meteorological tower to measure soil temperature (T_{soil}) at 0 cm, 5 cm, 10 cm, 15 cm, 20 cm, 30 cm, 40 cm, 50 cm, 70 cm, 80 cm, 100 cm, 150 cm, 160 cm, and 200 cm depth. The pF meter sensors also measured SWC at 10 cm, 20 cm, 40 cm, 80 cm, and 160cm depth.

All of above environmental parameters were synchronously monitored with eddy covariance, and the data was recorded every 30 minutes by CR3000 (Data logger, Campbell Data Taker Ltd, Salt Lake City, UT, USA). The air temperature sensors, the humidity sensors, and the pF meter sensors were calibrated in the State Key Laboratory of Frozen Soil Engineering at the Chinese Academy of Sciences in order to ensure the measurement accuracy was within ± 0.05 °C and ± 5%, respectively.

We also sampled soil profiles for soil physical and chemical measurements with one 1 meter × 1 meter × 2 meter pit 10 meter from the eddy covariance tower in August 2010. Five profile samples were taken from the pit at depths $0 - 20$ cm, $20 - 50$ cm, $50 - 120$ cm, $120 -$

160 cm, and 160 − 200 cm. Every depth was repeated five times after being fully mixed. Then each depth was stored in soil sample aluminum boxes and carefully sealed to prevent gas exchanges with air. The clod method was used to investigate the field wet bulk density (weight of soil per unit volume; Cate and nelson, 1971). The soil moisture content was calculated gravimetrically by the ratio of the mass of water present to the oven–dry (60 °C for 24 hour) weight of the soil sample. The soil organic carbon (SOC) content of the air–dried soil samples was analyzed using the wet combustion method, Walkley–Black modified acid dichromate digestion, $FeSO_4$ titration, and an automatic titrator. Total nitrogen (TN) and pH were measured using standard soil test procedures from the Chinese Ecosystem Research Network.

To understand the potential effect of soil thawing and freezing dynamics on CH_4 fluxes, we also reconstructed and verified semi-monthly data of soil active layer thickness (ALT). Following Muller's original definition, ALT is the maximum thaw depth in the late autumn using a linear interpolation of Tsoil profiles between two neighboring points above and below the 0 °C isotherm (Muller, 1947). We used records of the soil thawing thickness measured with a self–made geological probe to verify the ALT data semi–monthly. More information about the measurement procedure was previously described by Wu and Zhang (2010a).

2.4 Microbial Activity

To understand how soil microbial activity may have impacted the CH_4 fluxes, we sampled 100-gram soils for soil microbial activity measurements. These soils were obtained using a soil sample drill device (Ø=0.03 m), with depths of 0 − 25 cm taken every 5 days within 100 m of the eddy covariance tower. The sampled soil was fully mixed and divided into two equal parts. Each part was then stored in sterilized aluminum boxes and then placed in liquid nitrogen, before sending to the lab for microbe RNA extraction. We then used a real-time PCR method to

genetically test methanotrophic / archaeal methanogens, and the procedure was repeated three times for each sample. By setting the maximum methanotrophic / archaeal methanogens gene expression cyclic number as 1, we calculated the variety coefficient of methanotrophic and archaeal methanogens gene expressions (ΔI and ΔII, respectively; %) with equation (1):

$$\Delta_i = X_I / X_{Max} \quad \ldots \quad (1)$$

Δ_i is for the i[th] methanotrophic/archaeal methanogens gene expression; X_i is the methanotrophic / archaeal methanogen gene expression cyclic number of the i[th] time; X_{Max} is the maximum methanotrophic / archaeal methanogen gene expression cyclic number of the soil group from 2012 to 2016.

2.5 EC Data Processing and Data Filtering

Data collected from January 1st, 2012 to December 31st, 2016 was used in this study. Before processing, we removed data that was recorded at the time of precipitation events or with LI–7700 signal strength under 85. We first processed the raw data in Eddypro 6.2.0 (LI–COR, Lincoln, NE, USA). We adopted standardized procedures recommended in Lee et al. (2006) to process half–hourly flux raw measurements to ensure their quality.

1) Data was processed through statistical analysis in Eddypro 6.2.0 including: spike removal (accepted spikes < 5% and replaced spikes with linear interpolation), amplitude resolution (range of variation: 7.0 σ, number of bins: 100, accepted empty bins: 70%), drop–outs (percentile defining extreme bins: 10, accepted central drop–outs: 10%, accepted extreme drop–outs: 6%), absolute limits (-30 m s^{-1} < U < 30 m s^{-1}, -5 m s^{-1} < W < 5 m s^{-1}, -40 °C < Ts < 40 °C, 200 μmol

199 $mol^{-1} < CO_2 < 500$ µmol mol^{-1}, 0 µmol $mol^{-1} < H_2O < 40$ µmol mol^{-1}, 0.17 µmol $< CH_4 < 1000$
200 µmol), Skewness and kurtosis (-2.0 < Skewness lower limit < -1.0, 1.0 < Skewness up limit < 2.0;
201 1.0 < Kurtosis lower limit < 2.0, 5.0 < Kurtosis upper limit < 8.0), discontinuities (hard–flag
202 threshold: U = 4.0, W = 2.0, $T_S = 4.0$, $CO_2 = 40$, $CH_4 = 40$, and $H_2O = 3.26$; soft–flag threshold: U
203 = 2.7, W = 1.3, $T_S = 2.7$, $CO_2 = 27$, $CH_4 = 30$, and $H_2O = 2.2$), angle of attack (minimum angle of
204 attack = -30, maximum angle attack = 30, accepted amount of outliers = 10%), and steadiness of
205 horizontal wind (accepted wind relative instationarity = 0.5) (Vickers and Mahrt, 1997; Mauder et
206 al., 2013).

207 2) The data was then corrected using atmosphere physical calculations expressed by: axis
208 rotations of tilt correction (double rotation), time lags compensation (covariance maximization),
209 and compensating density fluctuations of Webb–Pearman–Leuning (WPL) terms. When CO_2 and
210 H_2O molar densities are measured with the LI–COR 7500 / LI–COR 7500A in cold environments
211 (low temperatures below -10 °C), a correction should be applied to account for the additional
212 instrument–related sensible heat flux, due to instrument surface heating / cooling. Thus, we
213 implemented the correction according to Burba et al. (2008), which involves calculating a
214 corrected sensible heat flux (H') by adding estimated sensible heat fluxes from key instrument
215 surface elements, including the bottom window (H_{bot}), top window (H_{top}), and spar (H_{spar})—to the
216 ambient sensible heat flux (H):

217 $$H' = H + H_{bot} + H_{top} + 0.15 \times H_{spar} \quad \ldots \quad (2)$$

218 3) Quality assurance (QA) / quality control (QC) were ensured through spectral analysis
219 and corrections analysis in Eddypro 6.2.0. Spectra and co–spectra calculations used power–of–two
220 samples to speed up the Fast Fourier Transform (FFT) algorithm. Spectra and co–spectra QA / QC

by filter were made according to Vickers and Mahrt (1997) test results, and Mauder and Foken (2004) micrometeorological quality test results. Low–frequency range spectral correction was done considering high–pass filtering effects. High–frequency range spectral correction was done considering low–pass filtering effects (Moncrieff et al., 2004).

4) We chose values "0","1", "2" to flag the processed flux data into three quality classes in Eddypro 6.2.0. The combined flag attains the value "0" for best quality fluxes, "1" for fluxes suitable for general analysis, such as annual budgets, and "2" for fluxes that should be discarded from the results dataset. For our dataset, approximately 67% of the data fell into Class 0, 12% in Class 1, and 21% in Class 2.

5) Our analysis indicated that, under average meteorological conditions, 80% of the flux (footprint) came from an area within 175 m of the eddy covariance tower.

In addition, we also adopted the method in Burba et al. (2008) to adjust the half–hour flux data, to avoid apparent measuring errors. In doing this, we rejected half–hour flux data that fell into one of the following situations: (1) incomplete half–hour measurements, (2) measurements under rain impacts, (3) nighttime measurements under stable atmospheric conditions (U*, friction velocity, < 0.1 m s^{-1}), and (4) abnormal values detected by a three–dimensional ultrasonic anemometer. This screening resulted in the rejection of about 20.7% of the flux data.

After the above data quality control, there was a 28.7% data gap for CH_4 fluxes over the entire exanimation period. These data gaps were then filled according to the method described in literature (Falge et al., 2001; Papale et al., 2003). We used a linear interpolation to fill the gaps if they were less than 2 hours, a method described in Falge *et al*. (2001) to fill gaps greater than 2 hours, but less than 1 day, and an artificial neural network approach as described in Papale et al.

(2003) and Dengel et al. (2013) to fill gaps greater than 1 day.

The quality of the dataset was evaluated using the equation of energy closure:

$$EBR = \sum(H + \lambda E) / \sum(R_n - G - S) \quad \ldots. \quad 3$$

where the *EBR* is surface energy balance ratio; *H* is heat flux; λE is latent heat; *Rn* is net radiation; *G* is soil heat flux (SHF); and *S* is heat storage of the vegetation canopy. As vegetation coverage at this research site is sparse, *S* is ignored. From 2012 to 2016, the *EBR* average was larger than 67.5%.

We analyzed two different major sources of CH_4 flux gap–filling uncertainty. The first kind of uncertainty came from U* threshold estimate. Following Burba et al. (2008), we excluded the probably false low CH_4 flux at low U*. However, it was difficult to determine the value for the U* threshold. For instance, when choosing a lower U* threshold, the associated lower flux would contribute to the gap filling and the annual gross (Loescher, et al., 2006). The variance from 5% to 95% of the bootstrapped values provided an average of the uncertainties caused by the U* to filter out. The second uncertainty source was due to insufficient power supply. In this research, all instrument power was supplied by solar. Extended periods of rainy, cloudy, and snowy weather, would cause the instrument to stop working due to an insufficient power supply. When we used the method to fill the gap mentioned above, it would cause the CH_4 to deviate from the true value. To our knowledge, the CH_4 flux data was largely uncertain under rainy conditions.

2.6 Based on microbial activities classification system of the four seasons

We redefined the four seasons of spring_, summer_, autumn_, and winter_, and based the parameters of the new seasons on microbial activities (Figure 2), ALT variety coefficients (ALT

variety coefficient = (ALT_{i+1} - ALT_i) / ALT_{Max}, where ALT_{Max} is the maximum of ALT per year), and Tsoil. Below, we describe the start date of each season (The end date of a season is the day immediately before the start of the next season).

Spring_ starts at the first day of two consecutive observation periods fulfilling both (1) ($\Delta II + \Delta I$) / 2 $\geqslant$ 15%, and (2) the ALT variety coefficient $\geqslant$ 0.05.

Summer_ starts on the first day of two consecutive observation periods when (1) ($\Delta II + \Delta I$) / 2 $\geqslant$ 45%, (2) ALT variety coefficient $\geqslant$ 0.35, and (3) five successive days with Tsoil at 40 cm soil depth $\geqslant$ 0 °C.

Autumn_ starts on the first day of two consecutive observation periods when (1) ($\Delta II + \Delta I$) / 2 $\geqslant$ 55%, (2) the ALT variety coefficient$\geqslant$ 0.60, and (3) five successive days the Tsoil of 10 cm $<$ 5 °C.

Winter_ starts on the first day of two consecutive observation periods that (1) ($\Delta II + \Delta I$) / 2 $<$ 15% and the ALT variety coefficient $<$ 0.05.

To test the robustness of our new seasonal division method in our methane cycle analysis, we compared empirical CH_4 flux estimates using different season definitions (Table 2). In addition to our new method that was based on top soil microbe activity, Tsoil of 0 – 40 cm, and permafrost active layer variability (hereafter refer to as SMT), we also used three conventional methods–one based on vegetation cover and temperature change (VCT), one on Julian months (JMC), and the other one on vegetation phenology change (VPC). Specifically, the VCT method splits a year into a plant growing season and a non–growing season; the JMC method assumes May to October as a plant growing season, and November to the following April as a non–

285 growing season; and the VPC method defines a plant growing season as the period between the
286 time when all dominant grass species (*Carex Moorcroft Falc. ex Boott, Kobresia tibetica Maxim,*
287 *Androsace tanggulashanensis, Rhodiola tibetica*) germinate and that when they all senesce.

288 **2.7 Statistical Analyses**

289 To understand the connections between CH_4 fluxes and associated environmental factors,
290 we performed a series of statistical analyses, including correlation, principal component analyses
291 (PCA), and linear regression analyses, in IBM SPSS (IBM SPSS Statistics 24; IBM, Armonk
292 NY, USA). Specifically, we used bivariate correlation to examine pairwise relationships between
293 environmental factors and CH_4 fluxes. We also used PCA and linear regressions to explore the
294 sensitivity of CH_4 fluxes to simultaneous environmental fluctuations in wind speed, Tair, air
295 relative humidity, Rn, vapor pressure deficit (VPD), albedo, SHF, SWC, and Tsoil. Before
296 performing PCA and linear regressions, the entire dataset was examined for outliers (Cook's
297 Distance, < 0.002), homogeneity of variance (Levene test, $p < 0.05$), normality (Kolmogorov–
298 Smirnov test, smooth line for histogram of Studentized residuals), collinearity (variance inflation
299 factor, $0 < VIF < 10$), potential interactions (*t*–test, $p < 0.05$), and independence of observations
300 (*t*–test, $p < 0.05$).

301 We performed structural equation modeling (SEM) to evaluate the effects of
302 environmental variables on CH_4 fluxes for different seasons. SEM is a widely-used multivariate
303 statistical tool that incorporates factor analysis, path analysis, and maximum likelihood analysis.
304 This method uses *priori* knowledge of the relationships between focus variables to verify the
305 validity of hypotheses. Here we performed SEM analyses with AMOS 21.0 (Amos Development
306 Corporation, Chicago, IL, USA). All data are presented as mean values with standard
307 deviations.

3. Results

3.1 Meteorological Conditions

We first reported the statistics of environmental factors at the Beilu'he Permafrost Weather Station based on meteorological records from 2012 to 2016. Mean annual Tair was -4.5 ℃ (Supplementary Figure 1), with minimum and maximum mean diel temperatures of -21.6 ℃ (12th January, 2012) and 13.8 ℃ (28th July, 2015), respectively. Average net radiation was 82.8 Wm^{-2}, while the maximum was in August (136.2 Wm^{-2}; Supplementary Figure 2). The average VPD was about 0.3, while the maximum was 0.98, and the minimum was 0.02 (Supplementary Figure 3). Mean annual precipitation was 335.4 mm (Figure 3), which was primarily based on rain and snowfall (only occupied 7%). From 2012 to 2016, the maximum precipitation was 2013 (488.3 mm), and the minimum was in 2015 (310.0 mm). The majority of precipitation, approximately 92%, occurred in the summer. During the winter, precipitation was rare and the mean value was about 6.7 mm, with the value decreasing even further from 14.2 mm in 2012, to 2.1 mm in 2016. Spring was another important rainfall period besides summer, with mean precipitation being about 37.5 mm, or 8～17% of the total.

The Beilu'he site is windy during most of the year (Supplementary Figure 4). Its annual average speed was 4.4 m s^{-1} from 2012 to 2016, while its maximum and minimum wind speeds were 14.6 m s^{-1} on 14th February, 2016 and 1.3 m s^{-1} on 1st November, 2013, respectively. Its winter, spring, and autumn average wind speed were 5.4 m s^{-1}, 4.3 m s^{-1}, and 3.7 m s^{-1}, respectively, while the principal direction of the strongest winds were from the southwest. Late autumn, winter, and early spring drought brought increased risks of dust blowing days, with an average of 122 days within a year. Its summer average wind speed was about 3.30 m s^{-1}, predominantly driven by the

southwest wind.

The SWC and Tsoil varieties of soil layers from 2012 to 2016 at the field site were summarized in Supplementary Figure 5 and Supplementary Figure 6, respectively. Mean SWC of depths 10 cm, 20 cm, 40 cm, 80 cm, and 160 cm were 14%, 9%, 8%, 14%, and 19%, respectively. Tsoil of depths 0 cm, 5 cm, 10 cm, 20 cm, 30 cm, 40 cm, 50 cm, 70 cm, and 80 cm corresponded with the Tair changes, but at depths 100 cm, 150 cm, 160 cm, and 200 cm did not correspond. The Tsoil of depth 200 cm had a remarkable difference from the Tsoil of other layers. The reason could be that peat existed in this layer, and that, during winter, the peat layer was not completely frozen. Supplementary Figure 7 shows SHF half-hour and diel scale varieties of 5 cm and 15 cm depth. The annual mean value of SHF at 5 cm and 15 cm depth is 7.6 Wm^{-2} and 6.8 Wm^{-2}, respectively.

Finally, we also reported the site's average soil freezing and thawing dynamics observed from January 2012 to December 2016 in Supplementary Figure 8. The duration of the active layer in the thawing state at 40 cm depth ranged from 174 to 188 days, with an average variation of up to 14 days. The average ALT is 4.4 m from 2012 to 2016.

3.2 Annual, Seasonal and Diel Variabilities of Methane Fluxes

Our results indicated that the Beilu'he site was a CH_4 sink, with an annual mean strength of -0.86 ± 0.23 g CH_4–C m^{-2} (95% confidence interval; negative values mean CH_4 sinks, positive values mean CH_4 sources). The strength of the CH_4 sink varies across different years from -0.57 ± 0.27g CH_4–C m^{-2} yr^{-1} in 2015, to -1.49 ± 0.38g CH_4–C m^{-2} yr^{-1} in 2014 (Figure 3). The amount of gene expression by methanogens and methanotrophs at 0 − 25 cm soils in March and November, for instance, were about 16.8% and 35.6%, respectively, suggesting strong microbial activities even during the cold and dry plant non–growing season (Figure 2).

We also clearly observed CH_4 seasonal variations (Supplementary Figure 9) in both the amount of CH_4 exchanges and their diel cycles (Figure 4). In winter_, the net CH_4 flux at the Beilu'he site was an atmospheric source, with an average annual rate of 0.41 ± 0.16 g CH_4–C m^{-2} yr^{-1} or 4.35 ± 0.33 mg CH_4–C m^{-2} d^{-1} (Supplementary Figure 9: a). It should also be noted that since the investigation started January 1st, 2012, and ended on December 31st, 2016, the 2011 ～ 2012 and 2016 ～ 2017 winters_ were only about half of the regular length. The diel CH_4 cycle of an average winter_ day was characterized by one single emission peak around 10:30am ～ 17:30 pm (Figure 4: a1, b1, c1, d1, e1 and f1).

In spring_, the Beilu'he site was a CH_4 source of 0.90 ± 0.37 g CH_4–C m^{-2} yr^{-1} (Supplementary Figure 9: b), accounting for 53% of annual CH_4 emissions, or 1.81 ± 0.22 mg CH_4–C m^{-2} d^{-1}. For a typical spring_ (Figure 4: a2, b2, c2, d2, and e2), diel CH_4 emission usually started at around 10:00 am ～ 10:30 am, when the thin ice layer on the soil surface started to thaw. It then reached the peak at 12:30 pm ～ 13:30 pm. The emission peak started to weaken at around 15:30 pm ～ 16:00 pm and reached around zero or even turned into a small sink after 20:00 pm.

In summer_, the Beilu'he site was a CH_4 sink of -0.99 ± 0.18 g CH_4–C m^{-2} yr^{-1} (Supplementary Figure 9: c), or -13.28 ± 0.38 mg CH_4–C m^{-2} d^{-1}. The diel cycle of CH_4 fluxes in summer_ was characterized with two absorption peaks and one small emission peak (Figure 4: a3, b3, c3, d3, and e3). With Tair increasing after sunrise, soils started to absorb atmospheric CH_4 and this soil uptake process reached its first peak at around 9:30 am ～ 10:30 am. After that, the continuously increasing Tair turned to suppress CH_4 uptake and promote CH_4 emissions, likely due to different temperature sensitivities of methanotrophic and methanogenic bacteria. At

around 15:30pm ~ 16:00 pm, when Tair reached the maximum (Supplementary Figure 1: b), CH_4 emission also reached its peak. The following temperature decrease in the late afternoon again reversed the CH_4 uptake / emission process, and by sunset we observed another CH_4 sink peak. The rate of CH_4 sink then decreased again through the night with further decreasing temperature.

Autumn_ was another season with a net CH_4 sink, with the season having the highest observed value for the site as a CH_4 sink in 2013 (Supplementary Figure 9: d). The CH_4 sink in autumn_ varied between -0.69 ± 0.19 g CH_4–C m^{-2} (2015), and -1.59 ± 0.33 g CH_4–C m^{-2} (2013), with an average diel rate of -1.19 ± 0.48 g CH_4–C m^{-2} yr^{-1} or -13.31 ± 0.28 mg CH_4–C m^{-2} d^{-1}. The diel dynamics of autumn_ CH_4 fluxes was like a letter "V", with a single sink peak during 13:30 pm ~ 15:30 pm (Figure 4: a4, b4, c4, d4, and e4).

3.3 Response of Methane Fluxes to Changes in Environmental Factors

Diel fluxes of CH_4 were highly correlated with many biotic and abiotic environmental factors, either positively or negatively (Table 3). Positive factors include metagenomics of both methanotrophic ($r = 0.52$, $p < 0.01$) and methanogens ($r = 0.49$, $p < 0.01$) at 0 − 25 cm soils, ALT ($r = 0.43$, $p < 0.01$), and wind speed ($r = 0.15$, $p < 0.01$). Important negative factors include VPD ($r = -0.26$, $p < 0.01$), SWC at all depths (varied r values between -0.17 and -0.26, $p < 0.01$), Tair ($r = -0.11$, $p < 0.01$), and air pressure ($r = -0.15$, $p < 0.01$). The correlation signal between CH_4 fluxes and Tsoil changed with soil depths (varied r values between -0.09 and 0.24, $p < 0.01$). Furthermore, path analysis results showed that Tsoil at 5cm and 10cm were the most important factors, which together contributed about 25% of the relative importance coefficient. Following these factors in importance were SWC at 80 cm (14%) and 20 cm (12%), and Tsoil at 20 cm (8%).

Further analyses suggested that dominant control factors of CH_4 fluxes also changed among different seasons. In spring_, Rn was the most important factor, with a relative importance coefficient near 60%, followed by SHF at 5 cm (9%), and SWC at 20 cm (6%). Table 4 shows the results of PCA. In spring_, PC1 explained 63% of the CH_4 variations, which was positively correlated with Tair, VPD, Rn, SHF of 15 cm, ALT, ΔI, SWC of 10 – 40 cm, Tsoil of 0 cm, Tsoil of 5 – 20 cm, Tsoil of 30 – 50 cm, and negatively correlated with wind speed. The PC2 explained about 23% of CH_4 fluxes variations. PC2 was positively correlated with wind speed, Tair, Rn, SHF of 15cm, but negatively correlated with VPD, ALT, ΔI, SWC 10 – 40 cm, Tsoil of 0 cm, Tsoil of 5 – 20 cm, and Tsoil of 30 – 50 cm. The first four principal components explained about 86% of the CH_4 variations.

In summer_, CH_4 fluxes were most related with Tsoil at 100 cm and 200 cm, with an relative importance coefficient of about 30.2% and 26.5%, respectively. Other important environmental determinants of CH_4 fluxes were Tsoil at 70 cm (12.3%), and Tsoil at 0 − 20 cm (11.4%). The first four principal components explained about 88% of the CH_4 variations (Table 4). PC1 explained 70% of the CH_4 variations. PC1 was positively correlated with wind speed, Tair, VPD, SHF of 15 cm, ALT, ΔI, SWC of 50 – 160 cm, precipitation, Tsoil of 0 cm, Tsoil of 5 – 40 cm, Tsoil of 50 – 80 cm, and Tsoil of 100 − 200 cm, but negatively correlated with Rn and SWC of 10 − 40 cm. PC2 was positively correlated with wind speed, Tair, VPD, Rn, SHF of 15cm, SWC of 10 − 40 cm, Tsoil of 0 cm, but negatively correlated with ALT, ΔI, SWC of 50 − 160 cm, precipitation, Tsoil of 5 − 40 cm, Tsoil of 50 − 80 cm, and Tsoil of 100 − 200 cm.

In autumn_, Rn and Tsoil at 5 − 20 cm had the highest relative importance coefficients for explaining the CH_4 flux variation. The first four principal components explained about 86% of the CH_4 variations (Table 4). PC1 explained 69% of the CH_4 variations. PC1 was positively

correlated with Tair, VPD, Rn, SHF of 15 cm, ALT, ΔI, SWC of 10 – 40 cm, SWC of 50 – 160 cm, Tsoil of 0 cm, Tsoil of 5 – 40 cm, Tsoil of 50 – 80 cm, and Tsoil of 100 – 200 cm, but negatively correlated with wind speed. PC2 was positively correlated with wind speed, Tair, Rn, SHF of 15 cm, ALT, ΔI, Tsoil of 0 cm, and Tsoil of 5 − 40 cm, but negatively correlated with VPD, SWC of 10 − 40 cm, SWC of 50 − 60 cm, Tsoil of 50 − 80 cm, and Tsoil of 100 − 200 cm.

During winter_, Rn was again the most important factor (34% relative importance coefficient), followed by Tsoil at 0 − 40 cm (27% in total), and SHF of 15 cm (17% in total), in determining CH_4 fluxes. The first four principal components explained about 96% of the CH_4 variations (Table 4). PC1 explained 75% of the CH_4 variations. PC1 was positively correlated with wind speed, Tair, VPD, Rn, SHF of 15 cm, ΔI, Tsoil of 0 cm, and Tsoil of 5 − 20 cm. PC2 explained 21% of the CH_4 variations. PC2 was positively correlated with wind speed, Tair, Rn, SHF of 15 cm, and ΔI, but negatively correlated with VPD, Tsoil of 0 cm, and Tsoil of 5 − 20 cm.

3.4 Empirical Model Comparison for Different CH_4 Flux Season Classification System

Lastly, we also compared how different season definitions, including the methods of SMT, VCT, JMC, and VPC, may have impacted the predictbility of CH_4 fluxes. We established empirical maximum likelihood models between all environmental factors and diel CH_4 fluxes over each season, and then compared modeled CH_4 fluxes and field observations under those methods of different seasonal definitions (Figure 5). We found that the agreement between modeled and observed CH_4 fluxes, using the new SMT method, reached $R^2 = 0.28$, almost twice that of the VPC ($R^2 = 0.17$) and VCT ($R^2 = 0.14$) methods, and more than three times that of the JMC method ($R^2 = 0.08$; Figure 5). Hence, the comparison suggested that our new method could better model CH_4 fluxes over a year. The use of the traditional plant growing season versus

nongrowing season definitions may also underestimate or overestimate CH_4 sinks or sources, especially when many studies assume CH_4 is close to zero during the plant nongrowing season. Furthermore, the new SMT method accurately captures the impact of spring_m and autumn_m permafrost thawing / freezing cycles on CH_4 fluxes, and the different preferable environments for methanogens and methanotrophic bacteria during the summer_m season, while conventional methods do not.

4. Discussion

4.1 Annual, Season mean and Diel Variability

Our results suggested that the alpine steppe ecosystem in Beilu'he was a CH4 sink of about -0.86 ± 0.23 g $CH_4 - C\ m^{-2}\ yr^{-1}$ during the study period of 2012-2016. This sink strength is larger than that of previous reports from other sites of the QTP (Cao et al., 2008; Wei et al., 2012; Li et al., 2012; Song et al., 2015; Chang and Shi, 2015), and many other high-latitude Arctic tundra ecosystems, like northeast Greenland (Jørgensen et al., 2015), western Siberia (Liebner et al., 2011), and Alaska (Whalen et al., 1992; Zhuang et al., 2004; Whalen, 2005). Different soil hydrothermal conditions, which previous studies have shown will greatly influence CH_4 cycles in permafrost regions (Spahni et al., 2011; Kirschke et al., 2013), may partly explain the site difference in CH_4 dynamics. For example, compared to the wet and often snow–covered high–latitude Arctic tundra ecosystems, there is no or little snow cover during the cold season in the QTP alpine steppes (Supplementary Table 1). During winter_, the Beilu'he meteorological data shows that the snow-cover time < 33.7h, SWC of 0-40cm within footprint < 7.6% from 2012 to 2016 (Supplementary Table 1) , is far below high–latitude Arctic tundra ecosystems. Jansson and Taş (2014) pointed out that relatively dry soils could faciliate the oxidation of CH_4, since the increased number of gaps between soil particles in dry soils enhances the diffusion of

oxygen (O_2) and CH_4 molecules and promotes aerobic respiration of soil microorganisms (Wang et al., 2014; Song et al., 2015). Meanwhile, unfrozen or capillary water found in cold–season permafrost soils ensures sufficient soil moisture for microbial activities, even in relatively drier and cold soils (Panikov and Dedysh, 2000; Rivkina et al., 2004). In addition, many previous studies used static chambers in CH_4 measurements, and may not have included a plant non–growing season (Wei et al., 2015a; Wang et al., 2014). Static chambers could underestimate CH_4 uptake because of the additional chamber heating-induced CH_4 emissions and frequent measurement gaps from overheating preventive shutdowns (Sturtevant et al., 2012).

We argued that seasonal freezing and thawing dynamics may be a key reason to explain the site's seasonal difference in CH_4 dynamics. Freezing and thawing processes are typical characteristics of the QTP permafrost (Wang et al., 2008; Wang et al., 2000; Qin et al., 2016). Our work suggests that freezing and thawing dynamics have played a critical role in governing permafrost seasonal and diel CH_4 cycling. For instance, while both spring_ and autumn_ are active seasons for the freeze-thaw dynamics of top soil layers and share many similarities, they have opposite CH_4 processes–soils emit CH_4 during spring_ (Supplementary Figure 9: b), but consume CH_4 during autumn_ (Supplementary Figure 9: d). We hypothesize that the difference in the freezing and thawing processes of the two seasons may have played a critical role in determining the direction of CH_4 dynamics. In spring_, the SWC of 10cm is 12.4%, 20-40cm is 9.2%, 80cm is 11.4%, and 160cm is 13.6% (Supplementary Table 1), the active soil layer thaws from top to bottom (Jin et al., 2000; Cao et al., 2017), and the permafrost table is very shallow (about 10 ～ 45 cm), and is generally water proof (Wu and Zhang, 2008; Song et al., 2015; Lin et al., 2015). The water thawed during the day time would freeze again at night on the soil surface (Supplementary Figure 10: a; Shi et al., 2006; Wu and Zhang, 2010b). The thin-ice layer

could stop atmospheric gases of CH_4 and O_2 from getting into the soils (Gazovic et al., 2010). During autumn_, the SWC of 10cm is 15.3%, 20-40cm is only 9.4%, but 80cm is 13.6%, and 160cm can up to 21.0% (Supplementary Table 1), however, soils are bidirectionally frozen from both top (ground surface) and bottom, the permafrost table, which is about 200~400 cm deep ; (Supplementary Figure 8; Wu and Zhang, 2010a), doesn't form a layer of thin ice during the nighttime surface soil freezing, because on the one hand, the frozen soil of the ground surface (about 0-40cm) prevents the outside liquid water from permeating. On the other hand, the freezing itself will reduce the liquid water content in the soil (Ma et al., 2015) Therefore, it creates finely closed anaerobic gaps that allow CH_4 and O_2 gases into deep soils (about 50~400cm; Mastepanov et al., 2008; Mastepanov et al., 2013; Zona et al., 2016). Meanwhile, the temperature of deep soils (about 50~400cm), still remains at a relatively high level (Supplementary Figure 10: b), and methanotrophic bacteria there are still active at this high Tsoil (Figure 2). This could be one important mechanism for autumn_ soil CH_4 consumption. In addition, in principal it was also possible that the observed seasonal variation in CH_4 flux may actually arise from the spatial variation of the footprint covered by the eddy covariance site (within 175m), given that prevalent wind direction changes seasonally (Supplementary Figure 4). Nonetheless, we found that the same vegetation species and soil exist in different directions to the tower within the footprint (Supplementary Figure 11). Hence this spatial vegetation and soil homogeneity further confirm that seasonal soil freezing and thawing differences may likely be the main explanation for seasonal CH_4 variations.

Furthermore, we suggested that the specific autumn_ soil vertical structure may help explain why the site was a CH_4 sink, unlike the CH_4 source in spring_. The sequential probing data enables us to establish a rough estimate on the soil vertical structure during the autumn_

thawing–freezing process, in which the vertical distribution of clay, sandy soils, and soil organic layers was mixed like a multi–layer hamburger structure, rather than forming a gradual change (Figure 6: e). As the soil profile has a different density, thermal conductivity, heat of phase transition, salinity of soil, and so on, we boldly conjecture that, similarly, the Tsoil, SWC, and soil microbial activities also had this hamburger type of vertical distribution. As a result, layers of frozen and thawed soils were not changing gradually but appeared like a hamburger structure too. This hamburger–like soil vertical structure trapped high concentrations of soil water between the frozen layers, which was therefore highly anaerobic and suitable for CH_4 production. Also, because of the hamburger–like structure, it fueled speculation that biogenic CH_4 between frozen layers could not escape in autumn_. The biogenic CH_4 was trapped until the ACL soil layer was completely frozen in late autumn_, and in some warmer years until early winter_ and created frost cracks. This enabled it to escape and may explain why there was a large burst of CH_4 emissions in late autumn_ and early winter_ and may also explain the constant weak CH_4 emission through the winter_ season, although methanogenic bacteria may have stopped functioning in the low temperature of winter_. Of course, this will need further study and necessitates direct data collection in the field.

4.2 Impacts of Environmental, Permafrost, and Microbial Activities on CH_4 Fluxes

Our results demonstrated the important roles of climate, freezing and thawing dynamics, and soil microbe activities in regulating the direction and amount of CH_4 exchanges between the atmosphere and ecosystems in permafrost areas. The key role of the above factors and processes was also confirmed by the better representation of seasonal CH_4 cycles by our new seasonal division method based on soil microbes, temperature, and permafrost dynamics rather than Tair or vegetation phenology. Here, we further discuss potential mechanisms of how environmental

(including air and soil heat and water), freezing and thawing processes, and soil microbes control the production and absorption of CH_4.

First, it is noteworthy that both the strength and direction of correlations between CH_4 fluxes, SWC, and Tsoil parameters changed with soil depths, particularly during spring_ and autumn_, when active layer soils shifted between thawing and freezing regularly. The positive and negative CH_4 flux correlations with Tsoil and SWC may suggest that the impacts of Tsoil and SWC on CH_4 fluxes shall be treated as a holistic process, rather than as separate ones. For instance, in autumn_, the correlation between CH_4 fluxes and Tsoil or SWC was positive at some soil depths, but negative at some other depths, reaching the maximum at the depth of 80 cm. Further, *in situ* observations suggested that soil organic matter and soil microbe amount were also at a very high level at this depth, highlighting that the regulation of soil abiotic factors on CH_4 cycling may be well influenced by soil biotic activities. In addition, the holistic soil heat–water process could also determine the concentration of soil inorganic ions, particularly during spring_ and autumn_, which were critical factors controlling the amount of soil unfrozen water. Soil unfrozen water in winter perhaps being important for maintaining soil microbial activities (Panikov and Dedysh, 2000; Rivkina et al., 2004); and in the future work we will include data acquiring of soil unfrozen water and test its role in regulating CH_4 exchanges in permafrost regions.

Tair and precipitation impact CH_4 fluxes indirectly through their influences on Tsoil and SWC (Zhuang et al., 2004; Lecher et al., 2015). Such indirect influences may often be characterized with time–lagged effects (Koven et al., 2011). For instance, post–drought rainfall events in summer_ can first promote soil CH_4 consumption (summer_ of 2014). This is because certain soil moisture is needed for methanogenic bacteria to function (Del et al., 2000; Luo et al.,

2012). Yet, prolonged rainfall will eventually cause CH_4 fluxes to change from negative (soils consume CH_4) to positive (soils emit CH_4) fluxes (for example, 168th to 183th of 2015, Figure 3: d). After rainfall events, CH_4 flux gradually turned negative again with the decrease of SWC. As a result of these time–lagged effects, the correlation coefficient between CH_4 fluxes and precipitation often appears very low, although still statistically significant.

Second, soil methanogenic and methanotrophic bacteria could co–exist with different optimal niches (e.g., ranges of Tair / Tsoil and SWC; Zhuang et al., 2013; Lau et al., 2015; Wei et al., 2015a). For example, the CH_4 diel cycle in summer_ was found to have two strong consumption peaks and one weak emission peak (Figure 4: a3, c3, d3, e3). The timing of these different peaks may well reflect the different environmental requirements for the dominance of methanogens and methanotrophic bacteria. Furthermore, methanogens may have a broader functional temperature range than methanotrophic bacteria (Kolb, 2009; Lau et al., 2015; Yang et al., 2016). This is also evident, for example, from the diel CH_4 cycle in autumn_ when CH_4 consumption was minimal at both lowest and highest Tair (Figure 4: a4, b4, c4, d4, e4).

The complex relationships between CH_4 fluxes and environmental factors make it a grand challenge to predict the future of the QTP CH_4 budget under a changing climate. For instance, it has been generally believed that the ALT will increase under projected warming (Wu and Liu, 2004). The positive correlation between CH_4 fluxes and ALT found here suggests that the QTP permafrost CH_4 sink may thus be weakened. However, the negative correlation between CH_4 flux and Tair may lead to a different conclusion. Incorporating our findings and high–resolution data into mechanistic CH_4 models is therefore needed to enhance our capacity in predicting future CH_4 budgets. Earth system models have been introduced to estimate CH_4 dynamics (Curry, 2007; Spahni et al., 2011; Bohn et al., 2015). For example, using a terrestrial ecosystem

modelling approach, Zhuang et al. (2004) estimated the average QTP permafrost CH_4 sink of -0.08 g C m^{-2} yr^{-1}, much smaller than our field–based CH_4 estimate (-0.86 ± 0.23 g CH_4–C m^{-2} yr^{-1}). Current CH_4 models focus on the regulation of CH_4 processes by temperature and SWC, and usually lack high–resolution data for model parameterization (Bohn et al., 2015). Data interpolation and the use of average values of certain environmental factors are normal practices in most models (Zhuang et al., 2004), which may overlook the impacts of environmental variations on CH_4 dynamics. For example, at Beilu'he, Tair on a typical summer day (e.g., July 6th, 2013) could vary between -6 °C and 28 °C, a difference of 34 °C. The resulting diel mean temperature, 17 °C, is beyond the range of methanotrophic bacteria's preferable temperature of 20～30 °C (Segers, 1998; Steinkamp et al., 2001; Yang et al., 2016). Therefore, models using diel mean temperature as an input may estimate the site as a net CH_4 sink. However, field observations show a source with a sink only during a short period (8:30am～11:30 am), on July 6th, 2013, because the short period of the sink was offset by the source over the remaining 21 hours. Furthermore, half–hourly SWC was well related with the waterproof role by the permafrost layer during spring_ and autumn_ (Figure 6: a). However, because of the shortage of high temporal resolution data, half–diel or diel mean SWC data are often used in many previous studies (Zhu et al., 2004; Jiang et al., 2010; Wei et al., 2015b), which could not correctly show the regulation of permafrost soil properties that are critical for CH_4 dynamics. As another example, Tsoil of 0 − 50 cm depth is one of the most important factors related to CH_4 fluxes (Mastepanov et al., 2008). However, many studies used Tair or re–analyzed deep Tsoil instead (Zhu et al., 2004; Bohn et al., 2015; Oh et al., 2016). Because the active layer is not homogeneous, but with different thermal conductivities during the freezing and thawing process, the use of Tair or deep Tsoil brings in large uncertainties in CH_4 modelling. Future research

needs to improve mechanistic understanding of CH_4 dynamics and their biotic and abiotic control factors, and to conduct more high–resolution and long–term field monitoring.

4.3 The Classification System of the Four Seasons for CH_4 Studies

Our study is also different from the majority of earlier studies in seasonal definitions (Treat et al., 2014; Wang et al., 2014; Wei et al., 2015a; Song et al., 2015). Here, we adopted a new classification system of the four seasons based on 0 − 25 cm soil depth bacterial activities (Figure 2), Tsoil of 0 − 40 cm (Supplementary Figure 6: a), and ALT (Supplementary Figure 8), rather than the conventional methods based on Tair and vegetation dynamics (Chen et al., 2011; McGuire et al., 2012). Previous studies indicated that changes in CH_4 fluxes are regulated by soil microbes, and activities of soil microbes are not limited to the warm season (Zhuang et al., 2004; Lau et al., 2015; Yang et al., 2016). For instance, in March and November, we found the amount of gene expression by methanogens and methanotrophs at 0 − 25 cm soils were about 16.8% and 35.6% (Figure 2), respectively, suggesting there are still strong microbial activities during the cold and dry season. Therefore, our new method of defining the four seasons from the top soil's biotic and abiotic features better captures the pattern of CH_4 dynamics throughout a year.

5. Conclusions

Our field data indicates that there was a large CH_4 sink in the QTP permafrost area during recent years. The strength of this CH_4 sink is larger than previous studies in the region and many high–latitude tundra ecosystems. This study highlights the complexity of environmental controls, including soil heat–water processes, permafrost freezing and thawing dynamics, and soil microbial activities, on CH_4 cycling. This complexity implies that linear interpolation and extrapolation from site-level studies could introduce large uncertainties in CH_4 flux estimation. Future quantification of CH_4 dynamics in permafrost regions needs to account for the effects of

627 complex environmental processes, including freezing and thawing, and the interaction between
628 heat and water, as well as microbial activities. Our findings also highlight the importance of
629 conducting more high–resolution and long–term field monitoring in permafrost regions for better
630 understanding and modelling of permafrost CH_4 cycling under a changing climate.

631 **Acknowledgements**

632 We would like to thank Yongzhi Liu, Jing Luo, Ji Chen, Guilong Wu, Wanan Zhu, Zhipeng
633 Xiao, and Chang Liao for their tremendous help in collecting field data over all these years. We
634 also want to pay tribute and gratitude to the late Xiaowen Cui for his contribution to our many
635 field adventures. We thank John McCabe for proofreading the manuscript. This study was
636 supported by the National Natural Science Foundation of China (41501083), Opening Research
637 Foundation of Key Laboratory of Land Surface Process and Climate Change in Cold and Arid
638 Regions, Chinese Academy of Sciences (LPCC201307), and Opening Research Foundation of
639 Plateau Atmosphere and Environment Key Laboratory of Sichuan Province (PAEKL − 2014 −
640 C3). A. C. acknowledges the support from a Purdue University Forestry and Natural Resources
641 research scholarship. The data generated in this study will be freely available on the Asia Flux
642 regional network server (https://db.cger.nies.go.jp/asiafluxdb/).

643 **Reference**

644 Bohn T., Melton J., Ito A.: WETCHIMP–WSL: intercomparison of wetland methane emissions
645 models over West Siberia, Biogeosciences, 12, 3321 – 3349, 2015.

646 Burba, G. G., Mcdermitt, D. K., and Grelle, A.: Addressing the influence of instrument surface
647 heat exchange on the measurements of CO_2 flux from open–path gas
648 analyzers. Glob. Change Biol., 14(8), 1854 – 1876, 2008.

649 Cao G., Xu X., and Long R.: Methane emissions by alpine plant communities in the Qinghai–
650 Tibet Plateau, Biol. Lett., 4, 681 – 684, 2008.

651 Cao B., Gruber S., Zhang T.: Spatial variability of active layer thickness detected by ground–
652 penetrating radar in the Qilian Mountains, Western China, J. Geophys. Res. Earth Surf.,
653 122, 574 – 591, 2017.

654 Cate, R. B., and Nelson, L. A.: A simple statistical procedure for partitioning soil test correlation
655 data into two classes, Soil Sci. Soc. Am. J., 35(4), 658 – 660, 1971.

656 Chang R., Miller C., and Dinardo S.: Methane emissions from Alaska in 2012 from CARVE
657 airborne observations, Proc. Natl. Acad. Sci. U. S. A., 111, 16694 – 16699, 2014.

658 Chang S. and Shi P.: A review of research on responses of leaf traits to climate change, Chin. J.
659 Plant Ecol., 39, 206 – 216, 2015.

660 Chen W., Wolf B., and Zheng X.: Annual methane uptake by temperate semiarid steppes as
661 regulated by stocking rates, aboveground plant biomass and topsoil air permeability.
662 Glob. Change Biol., 17, 2803 – 2816, 2011.

663 Curry C.: Modeling the soil consumption at atmospheric methane at the global scale. Glob.
664 Biogeochem. Cycles, 21, 1 – 15, 2007.

665 Dengel S., Zona D., and Sachs T.: Testing the applicability of neural networks as a gap–filling
666 method using CH_4 flux data from high latitude wetlands. Biogeosciences, 10, 8185 – 8200,
667 2013.

668 Del G., Parton W., and Mosier A.R.: General CH_4 oxidation model and comparisons of CH_4
669 oxidation in natural and managed systems, Glob. Biogeochem. Cycles, 14, 999 – 1019,

2000.

Falge, E., Baldocchi, D., and Olson, R.: Gap filling strategies for defensible annual sums of net ecosystem exchange, Agric. For. Meteorol., 107(1), 43 – 69, 2001.

Gažovič M., Kutzbach L., and Schreiber P.: Diurnal dynamics of CH_4 from a boreal peatland during snowmelt. Tellus, B, 62, 133 – 139, 2010.

IPCC, climate change 2013: the physical science basis. Contribution of working group I to the fifth assessment report of the intergovernmental panel on climate change., 2013.

Jansson, J. K. and Tas, N.: The microbial ecology of permafrost, Nat. Rev. Microbiol., 12, 414, 2014.

Jiang C., Yu G., and Fang H.: Short–term effect of increasing nitrogen deposition on CO_2, CH_4 and N_2O fluxes in an alpine meadow on the Qinghai–Tibetan Plateau, China, Atmos. Environ., 44, 2920 – 2926, 2010.

Jin H., Li S., and Cheng G.: Permafrost and climatic change in China, Glob. Planet, Change, 26, 387 – 404, 2000.

Jørgensen, C. J., Johansen, K. M. L., and Westergaard–Nielsen, A.: Net regional methane sink in High Arctic soils of northeast Greenland, Nat. Geosci., 8, 20, 2015.

Kirschke, S., Bousquet, P., and Ciais, P.: Three decades of global methane sources and sinks, Nat. Geosci., 6, 813, 2013.

Kolb, S.: The quest for atmospheric methane oxidizers in forest soils, Environ. Microbiol. Rep., 1, 336 – 346, 2009

Koven C.D., Ringeval B., and Friedlingstein P.: Permafrost carbon–climate feedbacks accelerate

global warming, Proc. Natl. Acad. Sci. U. S. A., 108, 14769 – 14774, 2011.

Lau M., Stackhouse B.T., and Layton A.C.: An active atmospheric methane sink in high Arctic mineral cryosols. ISME J., 9, 1880 – 1891, 2015.

Lecher A.L., Dimova N., and Sparrow K.J.: Methane transport from the active layer to lakes in the Arctic using Toolik Lake, Alaska, as a case study, Proc. Natl. Acad. Sci. U. S. A., 112, 3636 – 3640, 2015.

Lee, X., Massman, W., and Law, B. (Eds.): Handbook of micrometeorology: a guide for surface flux measurement and analysis (Vol. 29), Springer Science and Business Media, 2006.

Li K., Gong Y., and Song W.: Responses of CH_4, CO_2 and N_2O fluxes to increasing nitrogen deposition in alpine grassland of the Tianshan Mountains, Chemosphere, 88, 140 – 143, 2012.

Liebner S., Zeyer J., and Wagner D.: Methane oxidation associated with submerged brown mosses reduces methane emissions from Siberian polygonal tundra, J. Ecol., 99, 914 – 922, 2011.

Lin Z., Burn C.R., and Niu F.: The Thermal Regime, including a Reversed Thermal Offset, of Arid Permafrost Sites with Variations in Vegetation Cover Density, Wudaoliang Basin, Qinghai–Tibet Plateau. Permafr. Periglac. Process., 26, 142 – 159, 2015.

Loescher, H. W., Law, B. E., and Mahrt, L: Uncertainties in, and interpretation of, carbon flux estimates using the eddy covariance technique. J. Geophys. Res. Atmos., 111(D21), 2006.

Luo G.J., Brüggemann N., and Wolf B.: Decadal variability of soil CO_2, NO, N_2O, and CH_4 fluxes at the Höglwald Forest, Germany. Biogeosciences, 9, 1741 – 1763, 2012.

712 Mastepanov M., Sigsgaard C., and Dlugokencky E.J.: Large tundra methane burst during onset
713 of freezing. Nature, 456, 628 – 30, 2008.

714 Mastepanov, M., Sigsgaard, C., and Tagesson, T.: Revisiting factors controlling methane
715 emissions from high-Arctic tundra, Biogeosciences, 10(7), 5139, 2013.

716 Ma W., Zhang L., and Yang C.: Discussion of the applicability of the generalized Clausius–
717 Clapeyron equation and the frozen fringe process, Earth-Sci. Rev., 142, 47-59, 2015.

718 Mauder, M., Cuntz, M., and Drüe, C.: A strategy for quality and uncertainty assessment of long–
719 term eddy–covariance measurements. Agric. For. Meteorol., 169, 122 – 135, 2013.

720 McGuire A.D., Christensen T.R., and Hayes D.: An assessment of the carbon balance of Arctic
721 tundra: Comparisons among observations, process models, and atmospheric inversions,
722 Biogeosciences, 9, 3185 – 3204, 2012.

723 Moncrieff, J., Clement, R., and Finnigan, J.: Averaging, detrending, and filtering of eddy
724 covariance time series. In Handbook of micrometeorology (pp. 7 – 31), Springer
725 Netherlands, 2004.

726 Muller, S. W. Permafrost or permanently frozen ground and related engineering problems, 1947.

727 Oh Y., Stackhouse B., and Lau M.: A scalable model for methane consumption in arctic mineral
728 soils. Geophys. Res. Lett., 43, 5143 – 5150, 2016.

729 Panikov N.S. and Dedysh S.N.: Cold season CH_4 and CO_2 emission from boreal peat bogs (West
730 Siberia): Winter fluxes and thaw activation dynamics, Glob. Biogeochem. Cycles, 14, 1071
731 – 1080, 2000.

732 Papale, D., Reichstein, M., and Aubinet, M.: Towards a standardized processing of Net

733 Ecosystem Exchange measured with eddy covariance technique: algorithms and uncertainty
734 estimation. Biogeosciences, 3(4), 571 – 583, 2006.

735 Patra P.K. and Kort E.A.:Regional Methane Emission Estimation Based on Observed
736 Atmospheric Concentrations (2002 – 2012), J. Meteor. Soc. Japan. Ser. II, 94, 91 – 113,
737 2016.

738 Qin, Y., Wu T., and Li R., Using ERA-Interim reanalysis dataset to assess the changes of ground
739 surface freezing and thawing condition on the Qinghai–Tibet Plateau. Environ. Earth Sci.,
740 75(9): 1-13, 2016.

741 Rigby M., Prinn R.G., and Fraser P.J.: Renewed growth of atmospheric methane, Geophys. Res.
742 Lett.,35, 2 – 7, 2008.

743 Rivkina E., Laurinavichius K., and McGrath J.: Microbial life in permafrost, Adv. Space Res.,
744 33, 1215 – 1221, 2004.

745 Segers R.: Methane production and methane consumptiona–review of processes underlying
746 wetland methane fluxes [Review], Biogeochem., 41, 23 – 51, 1998.

747 Shi P., Sun X., and Xu L.: Net ecosystem CO_2 exchange and controlling factors in a steppe–
748 Kobresia meadow on the Tibetan Plateau. Sci. China Ser. D-Earth Sci., 49, 207 – 218, 2006.

749 Song, W., Wang, H., and Wang, G.: Methane emissions from an alpine wetland on the Tibetan
750 Plateau: Neglected but vital contribution of the non–growing season, J. Geophys. Res.
751 Biogeosci., 120, 1475 – 1490, 2015.

752 Spahni R., Wania R., and Neef L.: Constraining global methane emissions and uptake by
753 ecosystems. Biogeosciences, 8, 1643 – 1665, 2011.

754 Steinkamp R., Butterbach–Bahl K., and Papen H.: Methane oxidation by soils of an N limited
755 and N fertilized spruce forest in the Black Forest, Germany, Soil. Biol. Biochem., 33, 145 –
756 153, 2001.

757 Sturtevant C.S., Oechel W.C., and Zona D.: Soil moisture control over autumn season methane
758 flux, Arctic Coastal Plain of Alaska, Biogeosciences, 9, 1423 – 1440, 2012.

759 Treat C.C., Wollheim W.M., and Varner R.K.: Temperature and peat type control CO_2 and CH_4
760 production in Alaskan permafrost peats, Glob. Chang. Biol. 20, 2674 – 2686, 2014.

761 Vickers, D., and Mahrt, L.: Quality control and flux sampling problems for tower and aircraft
762 data. J. Atmos. Ocean. Technol., 14(3), 512 – 526, 1997.

763 Wang G., Li Y., and Wang Y.: Effects of permafrost thawing on vegetation and soil carbon pool
764 losses on the Qinghai–Tibet Plateau, China, Geoderma, 143, 143 – 152, 2008.

765 Wang S., Jin H., Li S.: Permafrost degradation on the Qinghai–Tibet Plateau and its
766 environmental impacts. Permafr. Periglac. Process., 11, 43 – 53, 2000.

767 Wang Y., Liu H., and Chung H.: Non–growing season soil respiration is controlled by freezing
768 and thawing processes in the summer monsoon-dominated Tibetan alpine grassland. Glob.
769 Biogeochem. Cycles, 28, 1081 – 1095, 2014.

770 Wei D., Ri X., and Wang Y.: Responses of CO_2, CH_4 and N_2O fluxes to livestock exclosure in an
771 alpine steppe on the Tibetan Plateau, China. Plant Soil, 359, 45 – 55, 2012.

772 Wei D., Ri X., and Tarchen T.: Considerable methane uptake by alpine grasslands despite the
773 cold climate: In situ measurements on the central Tibetan Plateau, 2008 – 2013, Glob.
774 Chang Biol., 21, 777 – 788, 2015a.

775 Wei D., Tarchen T., and Dai D.: Revisiting the role of CH_4 emissions from alpine wetlands on
776 the Tibetan Plateau: Evidence from two in situ measurements at 4758 and 4320 m above sea
777 level, J. Geophys. Res. Biogeosci., 120, 1741 – 1750, 2015b.

778 Whalen, S. C. and Reeburgh, W. S.: Consumption of atmospheric methane by tundra
779 soils. Nature, 346, 160, 1990.

780 Whalen S.C.: Biogeochemistry of Methane Exchange between Natural Wetlands and the
781 Atmosphere. Environ. Eng. Sci., 22, 73 – 94, 2005.

782 Whalen S.C., Reeburgh W.S., and Barber V.A.: Oxidation of methane in boreal forest soils: a
783 comparison of seven measures. Biogeochemistry, 16, 181 – 211, 1992.

784 Wu Q. and Liu Y.: Ground temperature monitoring and its recent change in Qinghai–Tibet
785 Plateau, Cold Reg. Sci. Technol., 38, 85 – 92, 2004.

786 Wu Q. and Zhang T.: Recent permafrost warming on the Qinghai–Tibetan Plateau. J. Geophys.
787 Res. Atmos. 113, 1 – 22, 2008.

788 Wu Q.and Zhang T.: Changes in active layer thickness over the Qinghai–Tibetan Plateau from
789 1995 to 2007, J. Geophys. Res. Atmos., 115, D09107, 2010a.

790 Wu Q. Zhang T., and Liu Y.: Permafrost temperatures and thickness on the Qinghai–Tibet
791 Plateau, Glob. Planet. Change, 72, 32 – 38, 2010b.

792 Yang S., Wen X., and Shi Y.: Hydrocarbon degraders establish at the costs of microbial richness,
793 abundance and keystone taxa after crude oil contamination in permafrost environments. Sci.
794 Rep., 6, 37473, 2016.

795 Zhu X., Zhuang Q., and Chen M.: Net exchanges of methane and carbon dioxide on the

Qinghai–Tibetan Plateau from 1979 to 2100. Environ. Res. Lett., 10, 85007. 2004.

Zhuang Q., Melillo J.M., and Kicklighter D.W.: Methane fluxes between terrestrial ecosystems and the atmosphere at northern high latitudes during the past century: A retrospective analysis with a process–based biogeochemistry model. Glob. Biogeochem. Cycles, 18(3), 2004.

Zhuang Q., Chen M., and Xu K.: Response of global soil consumption of atmospheric methane to changes in atmospheric climate and nitrogen deposition. Glob. Biogeochem. Cycles, 27, 650 – 663, 2013.

Zona D., Gioli B., and Commane R.: Cold season emissions dominate the Arctic tundra methane budget. Proc. Natl. Acad. Sci. U. S. A., 113, 40 – 45, 2016.

Table 1. Soil characteristics at the eddy covariance flux study site

Soil depth cm	Soil type	Gravel content g kg^{-1}	SOC g kg^{-1}	Microbial Numbers $\times 10^4$	pH	DBD g cm^{-3}	SWC %	Total N $\times 10^3$ mg kg^{-1}
0 − 20	clay	22.3	2.8	3.44	8.7	1.75	18.26	0.87
20 − 50	Silty clay	12.6	1.7	3.82	8.4	1.73	11.52	1.02
50 − 120	silt and fine sand	3.4	1.3	3.67	8.4	1.72	12.57	1.18
120 − 160	silt and fine sand	2.8	26.4	5.44	5.1	1.68	24.69	2.46
160 − 200	silt and fine sand	1.6	13.6	4.39	6.8	1.68	22.45	2.03

Note: Gravel content diameter ≥ 0.5cm. SOC is soil organic content, DBD is dry bulk density, and SWC is soil water content.

828 **Table 2.** Measurements of four seasons from 2012 to 2016

	Spring_ Period; Total days Days	Summer_ Period; Total days Days	Autumn_ Period; Total days Days	Winter_ Period; Total days Days	Plant growing season Period; Total days Days	Plant non–growing season Period; Total days Days
2012	50 − 142; 93	143 − 229; 87	230 − 323; 94	1 − 49, 324 − 366; 92	139 − 286; 148[a]	1 − 138, 287 − 366; 218[a]
					122 − 305; 184[b]	1 − 121, 306 − 366; 182[b]
					143 − 290; 148[c]	1 − 142, 291 − 366; 218[c]
2013	36 − 137; 102	138 − 224; 87	225 − 334; 110	1 − 35, 335 − 365; 66	139 − 287; 149[a]	1 − 138, 288 − 365; 216[a]
					121 − 304; 184[b]	1 − 120, 305 − 365; 181[b]
					127 − 297; 171[c]	1 − 126, 298 − 365; 194[c]
2014	49 − 127; 79	128 − 228; 101	229 − 309; 81	1 − 48, 310 − 365; 104	137 − 288; 152[a]	1 − 136 , 289 − 365; 213[a]
					121 − 304; 184[b]	1 − 120, 305 − 365; 181[b]
					142 − 294; 153[c]	1 − 141, 295 − 365; 212 [c]
2015	36 − 150; 115	151 − 224; 74	225 − 312; 88	1 − 35, 313 − 365; 88	145 − 288; 144[a]	1 − 144 , 289 − 365; 221[a]
					121 − 304; 184[b]	1 − 120, 305 − 365; 181[b]
					136 − 295; 160[c]	1 − 135, 296 − 365; 205[c]
2016	47 − 161; 115	162 − 225; 64	226 − 299; 74	1 − 46, 300 − 366; 113	141 − 287; 147[a]	1 − 140 , 288 − 366; 219[a]
					122 − 305; 183[b]	1 − 120, 305 − 366; 182[b]
					140 − 296; 157[c]	1 − 139, 297 − 366; 209[c]

Note: [a], based on vegetation cover and temperature change (VCT) (Lund et al., 2010; Tang and Arnone, 2013; Song et al., 2015); [b], based on Julian months (JMC) (Da et al., 2015); [c], based on vegetation phenology change (VPC). Spring_, Summer_, Autumn_, Winter_ are based on parameters of microbial activities, ALT variety coefficient and Tsoil (SMT).

844 **Table 3.** Correlation coefficients between CH_4 fluxes and environment factors on half–hour scales

	CH4 Flux									
Environment	Spring_		Summer_		Fall_		Winter_		2012 − 2016	
Factors	r	n	r	n	r	n	r	n	r	n
T_{air}	0.25**	24144	0.14**	19818	-0.16**	20959	0.32**	22224	-0.11**	87145
Wind Speed	0.31**	24144	-0.04**	19817	-0.20**	20959	0.32**	22224	0.15**	87144
VPD	-0.33**	18624	-0.21**	19263	-0.09**	16737	-0.21	18000	0.26**	69624
Rn	0.55**	24143	0.09**	19807	-0.33**	20913	0.51**	22224	0.09**	87087
Albedo	0.07**	24144	-0.01	19814	-0.08**	20913	0.10**	22224	0.02**	87095
SHF of 5cm	0.46**	24144	-0.08**	19818	-0.23**	20913	0.43**	22224	0.09**	87099
SHF of 15cm	0.36**	24144	-0.15**	19815	-0.23**	20913	0.33**	22224	0.08**	87096
SWC of 10cm	-0.16**	24144	-0.14**	19818	-0.06**	20959	0.00	22224	-0.25**	87145
SWC of 20cm	-0.15**	24144	-0.13**	19816	-0.07**	20959	0.11**	22224	-0.24**	87143
SWC of 40cm	-0.11**	24144	-0.02**	19818	0.07**	20959	0.06**	22224	-0.17**	87145
SWC of 80cm			-0.13**	19818	0.06**	20959				
SWC of 160cm			0.04**	19818	-0.11**	20959				
Precipitation			-0.02	16748	0.01[b]	17888				
ALT	0.73**	23004	0.23**	19823	0.73**	21454			0.43**	64281

ΔI	0.77**	100	0.57**	83	0.46**	89	0.23	93	0.49**	365
ΔII	0.31**	100	0.66**	83	0.78**	89	0.19	93	0.52**	365
T_{soil} of 0 cm	-0.06*	23004	0.13**	19823	0.07**	20366	0.13**	21711	0.11**	84904
T_{soil} of 5 cm	0.15**	24144	0.15**	19808	-0.13**	21454	0.27**	22224	0.24**	87630
T_{soil} of 10 cm	-0.03**	24144	0.12**	19808	0.08**	21454	0.16**	22224	0.13**	87630
T_{soil} of 20 cm	-0.14**	24144	0.08**	19808	0.02**	21454	0.06**	22224	-0.09**	87630
T_{soil} of 30 cm	-0.13**	23004	0.06**	19823	-0.02**	20366	0.07**	21711	-0.08**	84904
T_{soil} of 40 cm	0.14**	24144	0.05**	19808	-0.01[b]	21454	0.06**	22224	0.11**	87630
T_{soil} of 50 cm			0.04**	19823	-0.05**	20366				
T_{soil} of 70 cm			0.07**	19823	-0.05**	20366				
T_{soil} of 80 cm			0.05**	19808	0.04**	21454				
T_{soil} of 100 cm			0.10**	19823	-0.05**	21454				
T_{soil} of 150 cm			0.09**	19823	-0.04**	20366				
T_{soil} of 160 cm			0.10**	19808	0.01**	21454				
T_{soil} of 200 cm			0.02**	19823	-0.02**	20366				

Note: ** means $p<0.01$, * means $p<0.05$; r values for the relationship between CH_4 flux and environment factors. Tair means air temperature of 3 m above the ground surface. VPD is vapor pressure deficit, NR is net radiation, and SWC is soil water content, ALT is active layer thickness, which fitted through the depth of soil 0 ℃ in Surfer 8.0., and the data is removed as meaningless in winter. Tsoil is the temperature of the soil. In spring_ and

848 winter_, precipitation data is too sparse for statistical analysis. ΔI is the soil 0 − 25cm archaeal methanogens gene expression, and ΔII is the soil 0 − 25
849 cm methanotrophic gene expression. The coefficients (r) between CH_4 flux and ΔI, ΔII are obtained using the synchronous CH_4 fluxes averaged for 5
850 days.

851

852

853

854

855

856

857

858

859

860

861

862 **Table 4**. Principal components analysis (PCA) of the environmental factors.

	Spring_				Summer_				autumn_				Winter_			
Component	PC1	PC2	PC3	PC4	PC1	PC2	PC3	PC4	PC1	PC2	PC3	PC4	PC1	PC2	PC3	PC4
wind speed	-0.03	0.51	0.65	-0.46	0.02	0.37	0.38	-0.13	-0.04	0.44	0.59	0.67	0.27	0.45	-0.11	-0.27
Tair	0.38	0.29	-0.05	-0.11	0.42	0.22	-0.03	0.02	0.36	0.21	0.08	-0.06	0.48	0.12	-0.02	0.01
VPD	0.34	-0.27	0.40	0.15	0.17	0.46	-0.22	0.09	0.34	-0.15	0.17	-0.07	0.14	-0.15	0.95	-0.22
Rn	0.16	0.49	0.00	0.76	-0.01	0.07	0.58	0.11	0.12	0.54	-0.43	-0.07	0.26	0.47	-0.01	-0.49
SHF of 15cm	0.24	0.49	-0.30	-0.09	0.25	0.53	-0.09	0.01	0.15	0.59	-0.23	-0.15	0.36	0.37	0.14	0.58
ALT	0.22	-0.40	0.40	0.27	0.32	-0.53	-0.05	0.02	0.29	0.49	0.70	0.25				
ΔI	0.49	-0.22	0.01	-0.08	0.50	-0.16	0.02	-0.16	0.29	0.31	0.24	-0.51	0.52	0.05	0.07	-0.03
SWC of 10 − 20cm													-0.31	0.45	0.22	0.47
SWC of 10 − 40cm	0.33	-0.20	0.50	0.25	-0.16	0.15	-0.16	0.73	0.28	-0.18	-0.41	0.53				
SWC of 50 − 160cm					0.23	-0.20	-0.16	0.55	0.31	-0.17	-0.32	0.41				
Precipitation					0.03	-0.04	0.63	0.35								
Tsoil of 0 cm	0.43	-0.07	-0.20	-0.27	0.43	0.08	0.08	-0.07	0.37	0.07	0.19	-0.16	0.43	-0.35	-0.15	0.09
Tsoil of 5 − 20 cm	0.44	-0.01	-0.17	-0.16									0.45	-0.28	0.00	0.28
Tsoil of 5 − 40 cm					0.46	-0.05	0.04	-0.03	0.38	0.02	0.18	-0.17				
Tsoil of 30 − 50cm	0.40	-0.23	-0.08	-0.04												
Tsoil of 50 − 80cm					0.37	-0.36	0.00	0.01	0.37	-0.11	0.19	-0.14				
Tsoil of 100 − 200cm					0.33	-0.34	0.01	-0.01	0.36	-0.14	0.08	0.00				
Percent of variance	0.63	0.23	0.08	0.04	0.70	0.18	0.07	0.02	0.69	0.17	0.08	0.04	0.75	0.21	0.02	0.01
Cumulative	0.63	0.86	0.94	0.98	0.70	0.88	0.95	0.97	0.69	0.86	0.94	0.98	0.75	0.96	0.98	0.99

863 **Note:** PC means principal component. Before PCA, SWC was divided for three parts, 10 – 20 cm, 10 – 40 cm, and 50 – 160 cm according to collinearity
864 test in four seasons. Tsoil was divided for six parts of Tsoil of 0 cm, Tsoil of 5 – 20 cm, Tsoil of 5 – 40 cm, Tsoil of 30 – 50 cm, Tsoil of 50 – 80 cm,
865 and Tsoil of 60 – 200 cm according to collinearity test in different seasons.

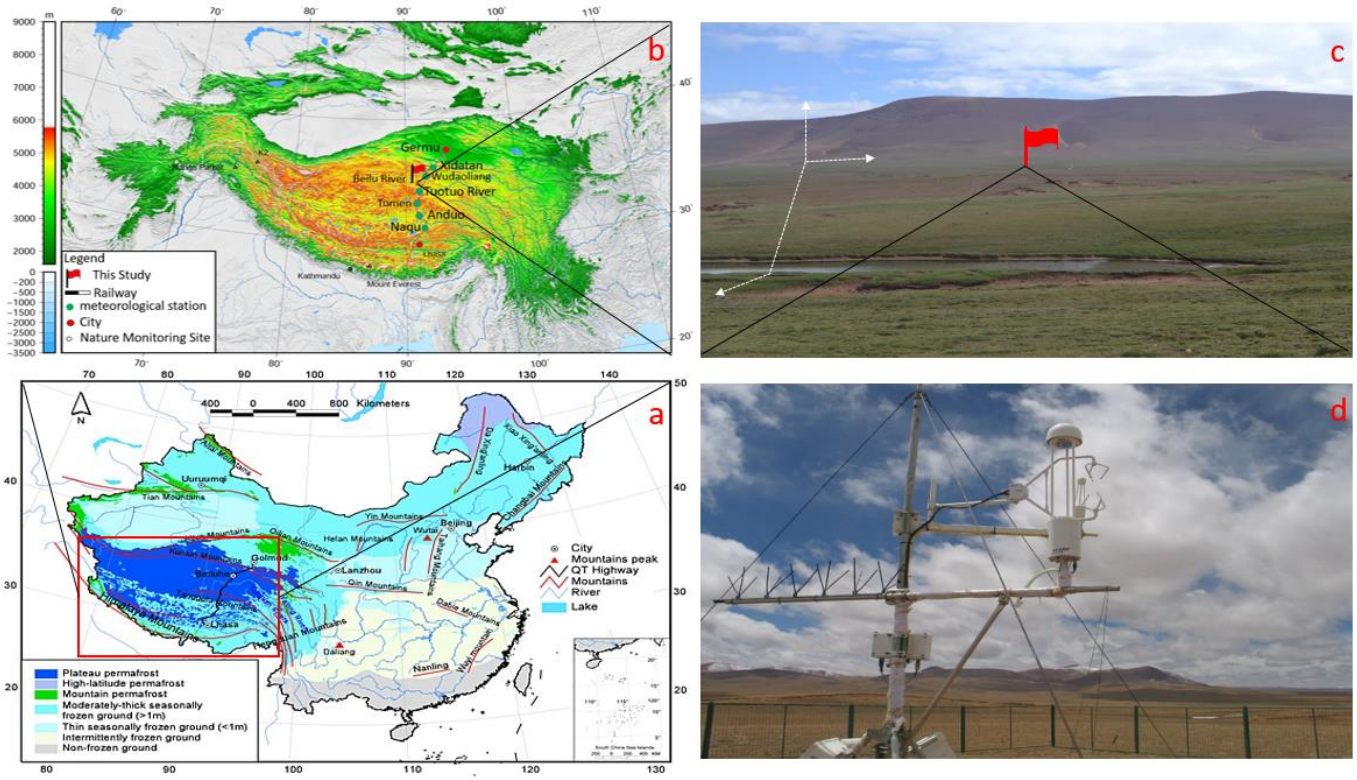

Figure 1. Geographic location of the study site: (a) is a map of China's permafrost distribution, and the red box marks the approximate location of the Qinghai–Tibet Plateau; (b) shows the study site location and meteorological stations along the Qinghai–Tibet railway; (c) is the photo showing the study site's topography and physiognomic. The small red flag in (c) is the eddy covariance tower location; (d) is the close–up shot of the LI–7700 for methane measurement. *Map boundary and location are approximate. Geographic features and the names do not imply any official endorsement or recognition*

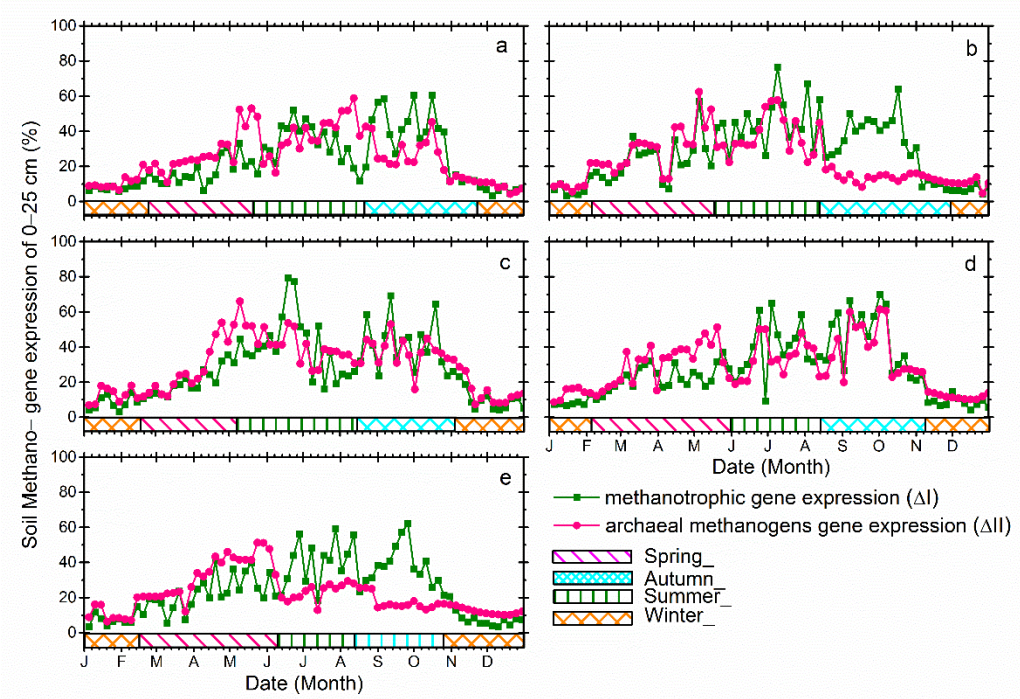

Figure 2. Annual patterns of soil methanogen−gene expression of 0 − 25 cm soil depth for years: (a) 2012, (b) 2013, (c) 2014, (d) 2015, and (e) 2016.

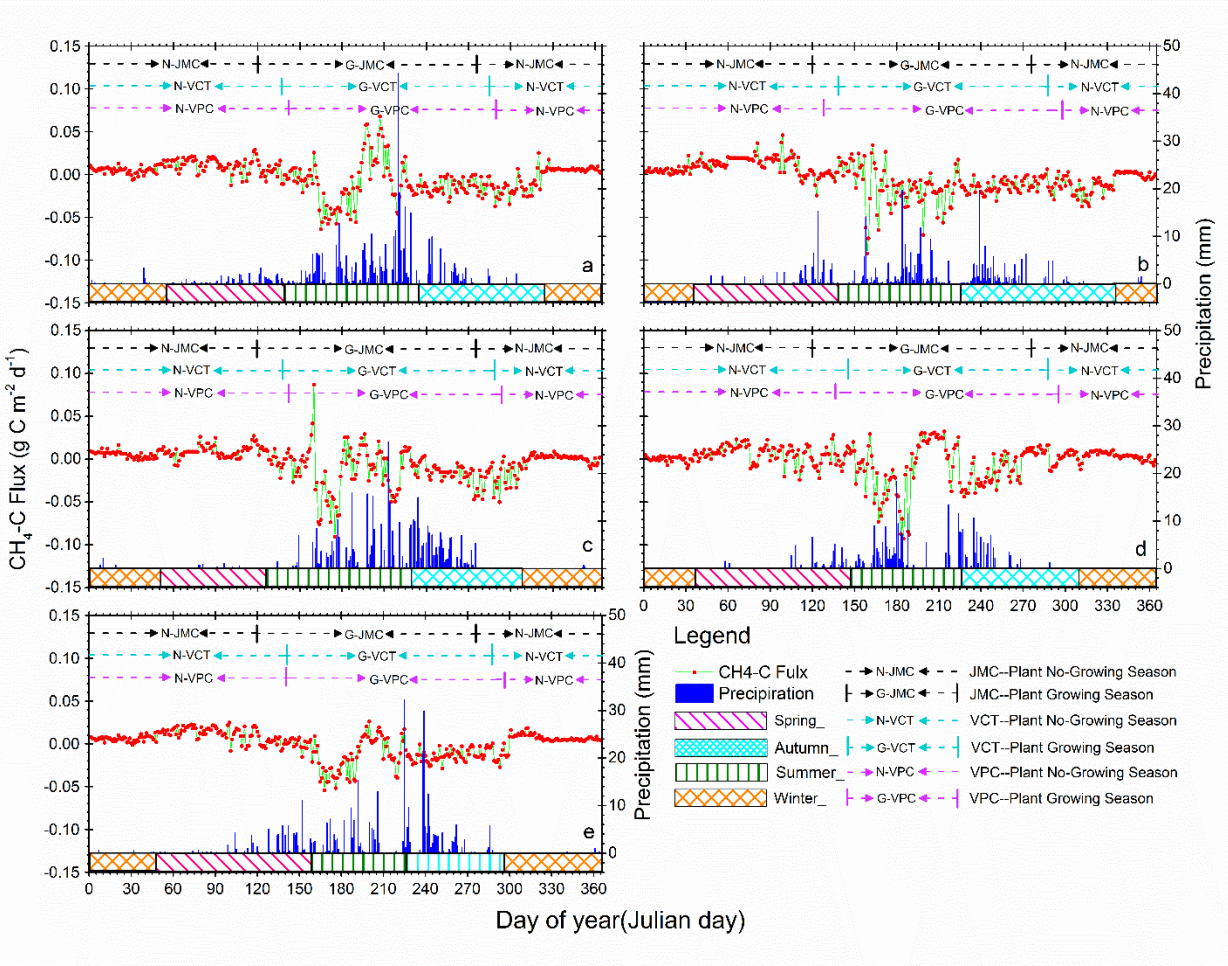

883

884 **Figure 3.** Annual patterns of diel methane (CH_4) flux and precipitation variations from 2012 to 2016. Positive values indicate CH_4 release and
885 negative values indicate CH_4 uptake by ecosystems. Red dots and light green lines are CH_4–C flux variation, and the deep blue histograms show diel
886 precipitation accumulation. Pink, olive, cyan, and orange blocks mean spring, summer, autumn, and winter seasons respectively, according to our
887 new method of SMT (see Methods), . Black, cyan, and pink dotted lines with bars separated the plant growing from non–growing seasons and stand
888 for seasons by the method JMC, VCT, and VPC, respectively. Details about the methods JMC, VCT, and VPC can be found in Text part 3.2.

889

890

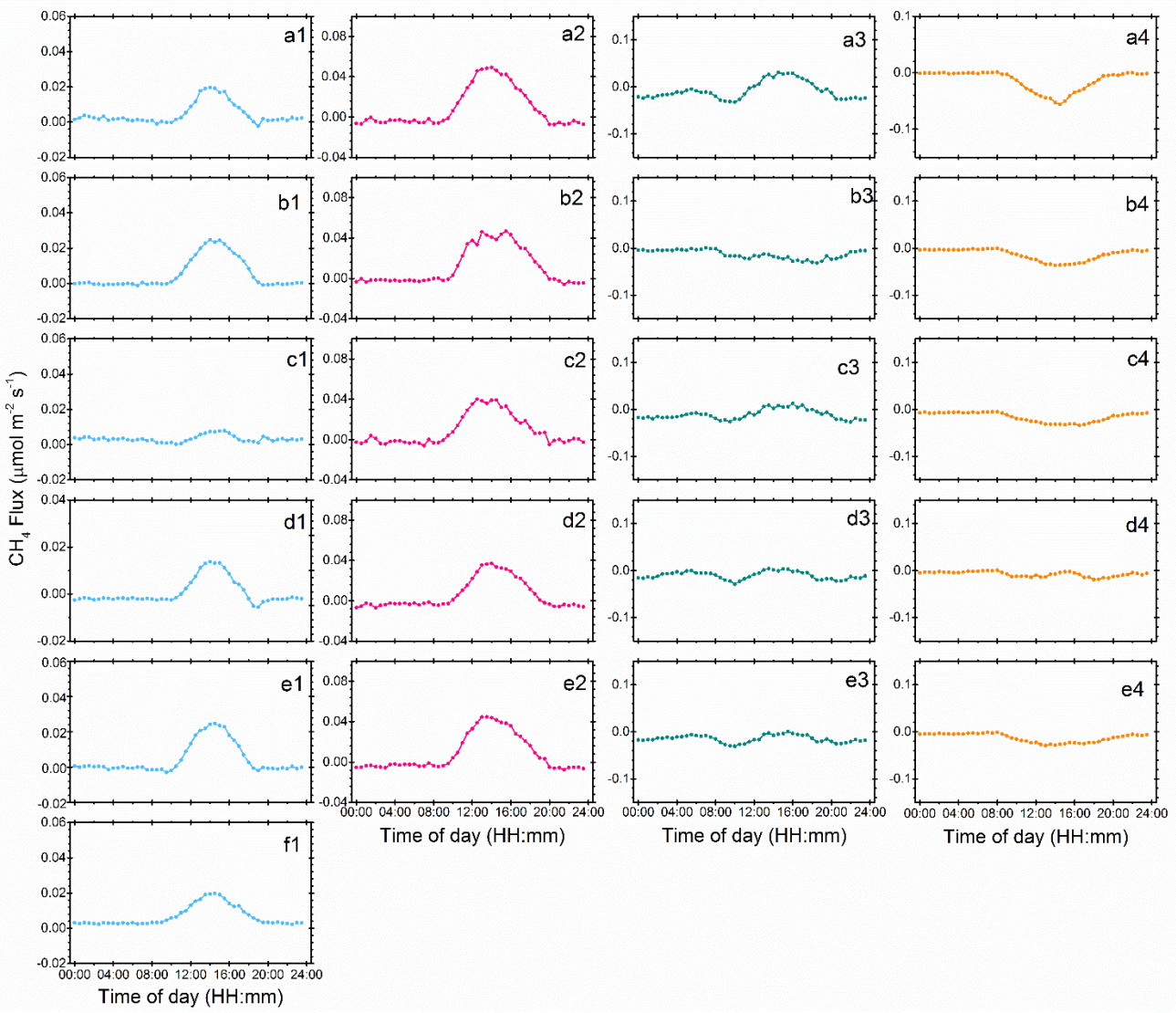

Figure 4. Diel CH_4 fluxes from 2012 to 2016 for different seasons. Blue, pink, green and orange, represent winter, spring, summer, and autumn, respectively; (a1), (a2), (a3), and (a4) are for 2012; (b1), (b2), (b3), and (b4) are for 2013; (c1), (c2), (c3) and (c4) are for 2014; (d1), (d2), (d3), and (d4) are for 2015; (e1), (e2), (e3), (e4) and (f1) are for 2016.

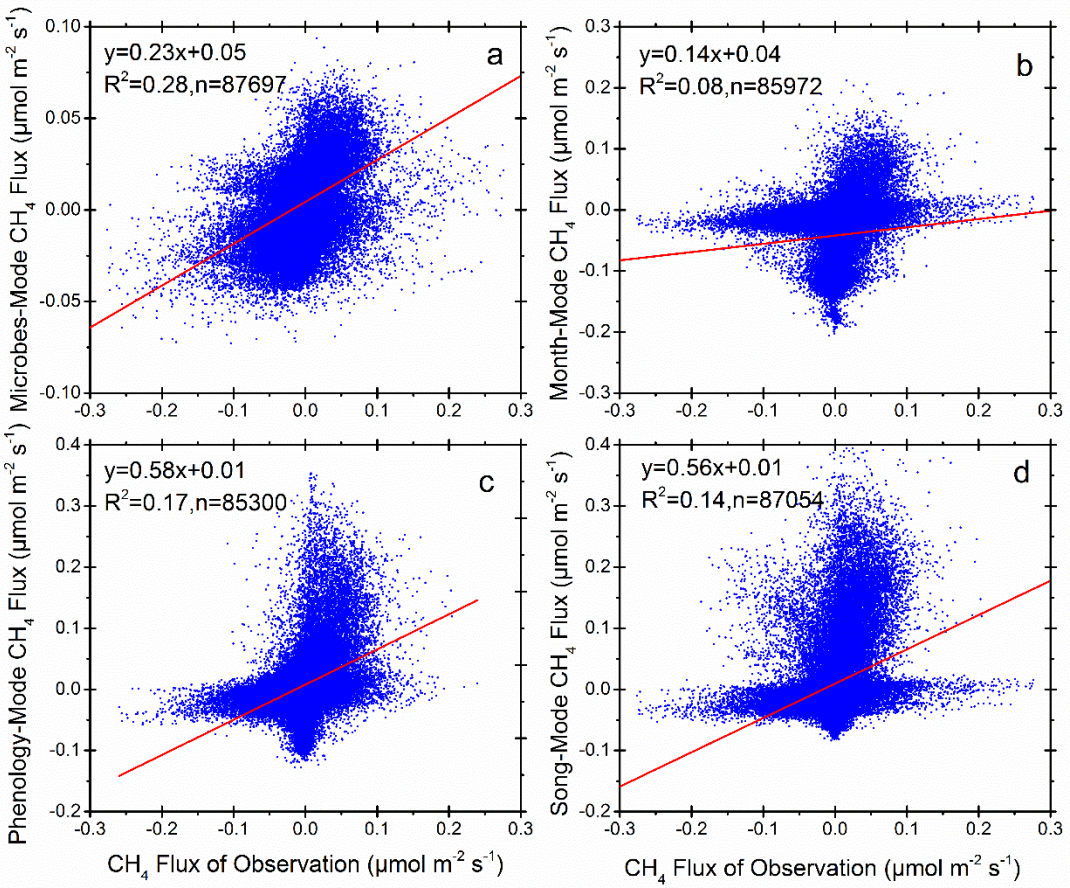

Figure 5. Regression comparison between observation and modeled methane fluxes with four different seasonal definitions and classification models. Panels (a), (b), (c), and (d) are for the SMT, JMC, VCT, and VPC methods, respectively.

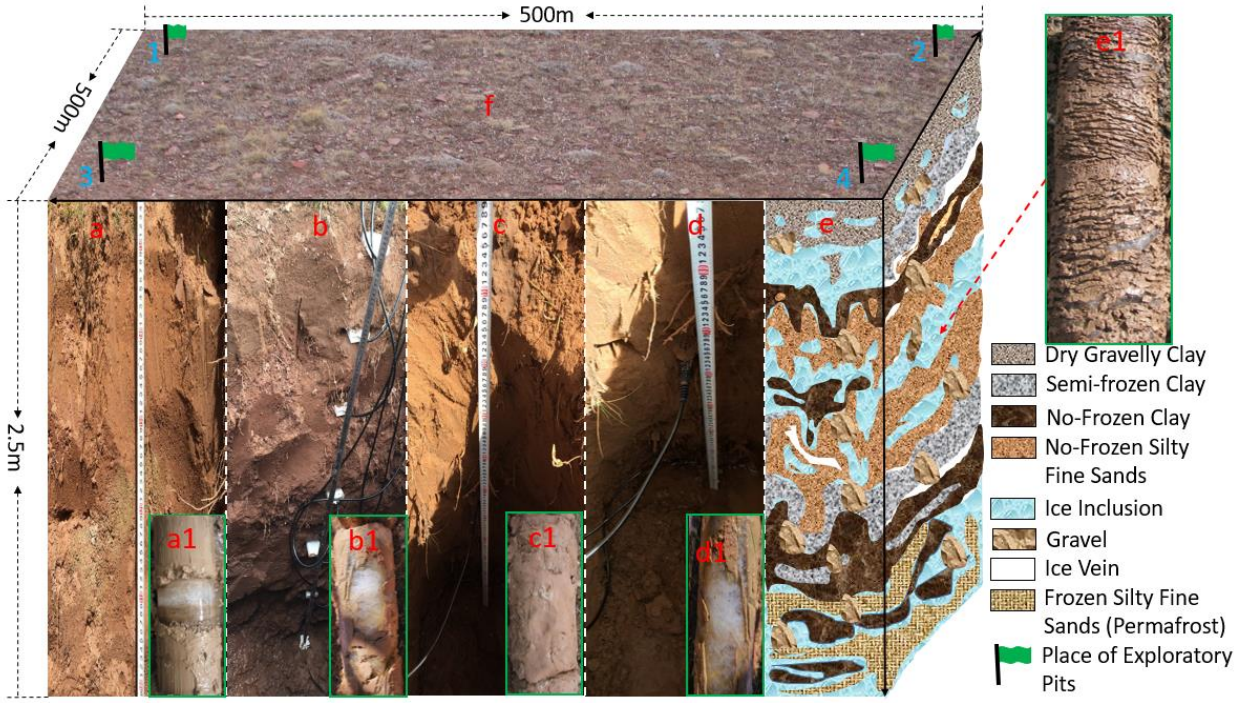

Figure 6. Location of exploratory pits and drillings in this study in autumn: (f) is photo of a typical ground surface (October 16th, 2014). Green flags represent the location for the soil survey by test pitting and drilling. (a), (b), (c), and (d) are test pitting sections for active layer 0 − 250 cm depths soil water content and temperature measured in eddy covariance North (1), South (2), East (3), and West (4) corners, respectively. (a1), (b1), (c1), and (d1) are drilling cores, with clear ice (white) in (a1), (b1), and (d1), but not in (c1); (e) provides an illustration that combines results from drillings, test pitting and multi–channel ground–penetrating radar (Malå Geoscience, Sweden) for active layer variations in permafrost area during the autumn season; and (e1) is a core sample of the same drilling (October 16th, 2014).

Supplement

Supplementary Table 1 Seasonal soil water content (SWC, %) of winter_, spring_, summer_, and autumn_ from 2012 to 2016.

Seasonal	Period	10 cm	20 cm	40 cm	80cm	160cm
		Soil Water Content (SWC), %				
Winter_	2012 early	0.11	0.08	0.07	0.11	0.14
	2012-2013	0.10	0.08	0.07	0.11	0.16
	2013-2014	0.10	0.08	0.07	0.11	0.13
	2014-2015	0.10	0.08	0.07	0.11	0.17
	2015-2016	0.10	0.08	0.07	0.11	0.16
	2016 later	0.10	0.08	0.07	0.12	0.19
	Average	0.10	0.08	0.07	0.11	0.16
Spring_	2012	0.13	0.09	0.08	0.11	0.13
	2013	0.12	0.09	0.08	0.11	0.13
	2014	0.12	0.08	0.07	0.11	0.13
	2015	0.13	0.09	0.08	0.11	0.14
	2016	0.12	0.09	0.08	0.13	0.15
	Average	0.12	0.08	0.08	0.11	0.14
Summer_	2012	0.18	0.11	0.10	0.17	0.27
	2013	0.16	0.11	0.11	0.19	0.25
	2014	0.16	0.10	0.10	0.16	0.24
	2015	0.16	0.10	0.10	0.19	0.28
	2016	0.16	0.10	0.09	0.18	0.28
	Average	0.17	0.10	0.10	0.18	0.26
Autumn_	2012	0.14	0.09	0.08	0.14	0.21
	2013	0.14	0.09	0.09	0.15	0.20
	2014	0.16	0.10	0.10	0.16	0.22
	2015	0.15	0.10	0.09	0.15	0.21
	2016	0.16	0.10	0.09	0.16	0.21
	Average	0.15	0.10	0.09	0.15	0.21

913

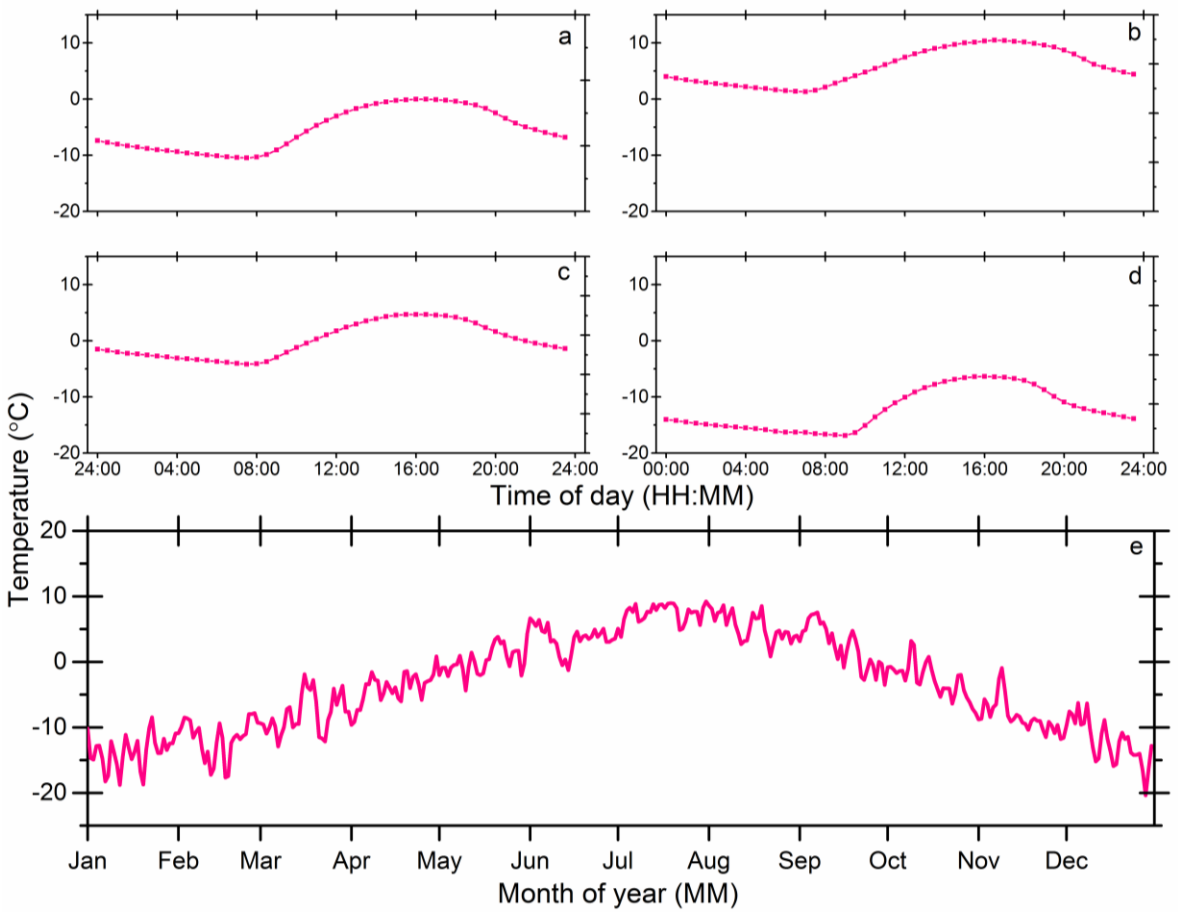

914

915 **Supplementary Figure 1.** Air temperature (Tair) of 3 meters above the ground surface: (a), (b),

916 (c), and (d) are half–hour scale mean values in spring, summer, autumn, and winter, respectively;

917 (e) shows diel–scale mean values from 2012 to 2016.

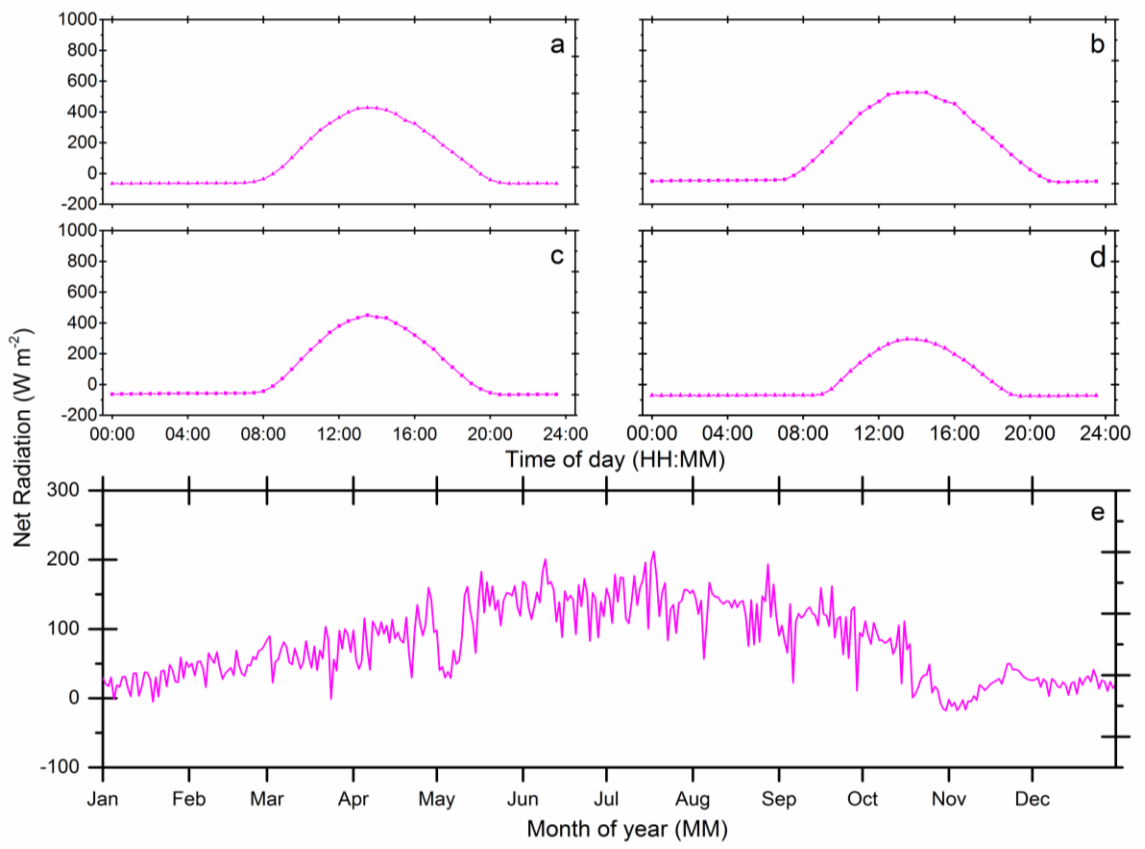

Supplementary Figure 2. Net radiation (Rn) of 3 meters above the ground surface: (a), (b), (c), and (d) are half–hour scale mean values in spring, summer, autumn, and winter, respectively; (e) shows diel–scale mean values from 2012 to 2016.

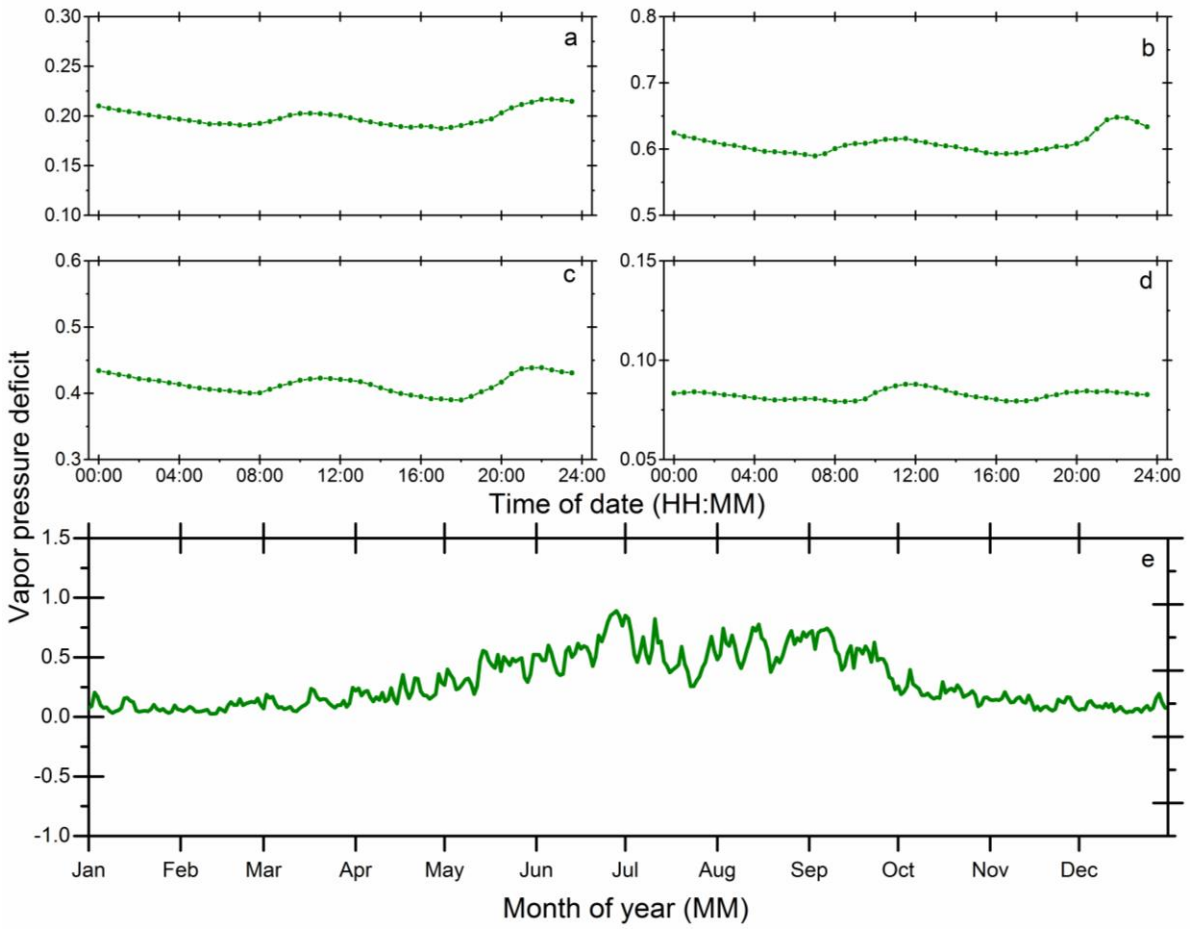

923

924 **Supplementary Figure 3.** Vapor pressure deficit (VPD) of 3 meters above the ground surface:

925 (a), (b), (c), and (d) are half–hour scale mean values in spring, summer, autumn, and winter,

926 respectively; (e) shows diel–scale mean values from 2012 to 2016.

927

928

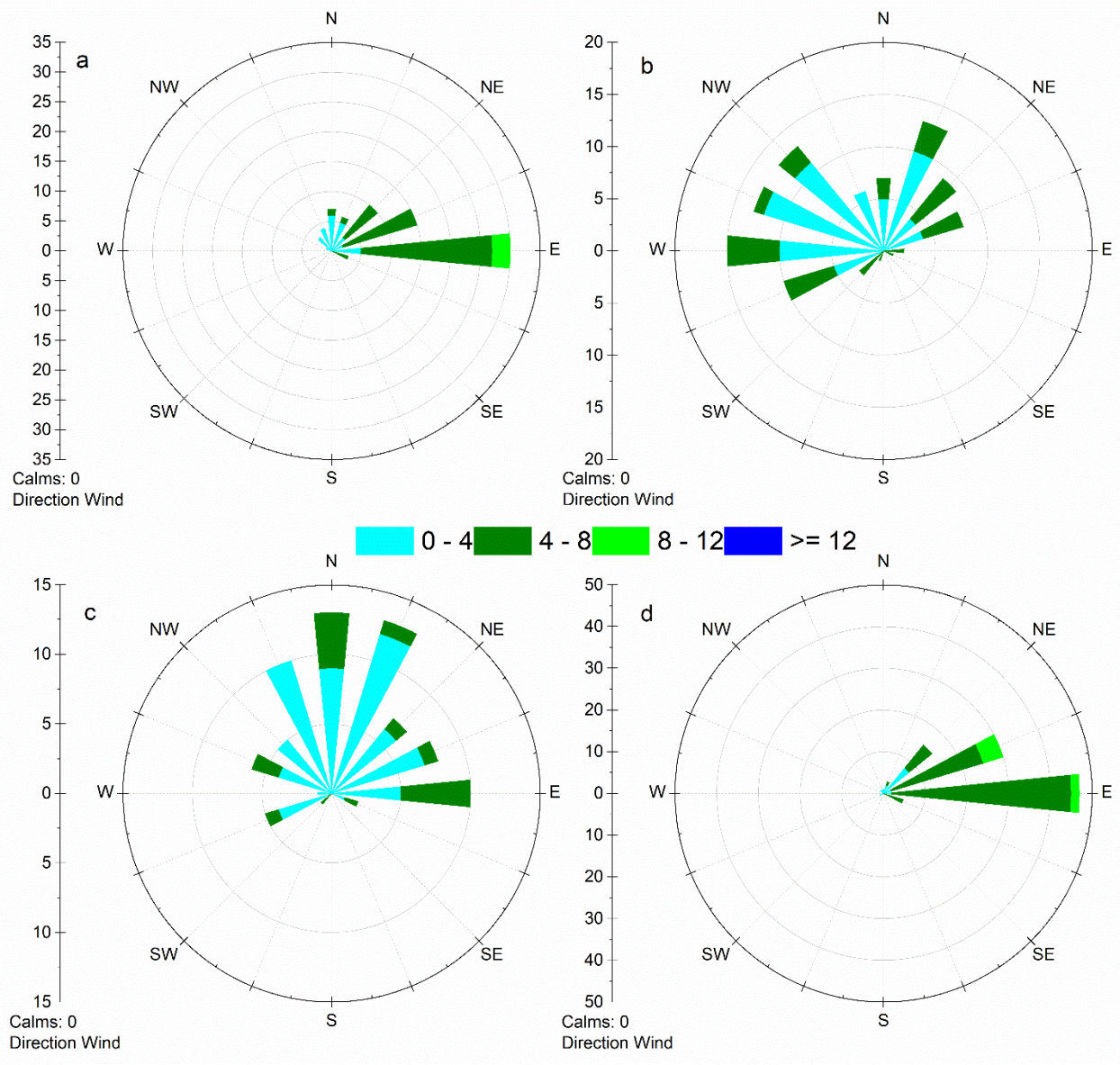

Supplementary Figure 4. Diel mean of wind speed and direction between 2012 and 2016. All data are presented as mean values with standard deviations (mean ± standard deviation).

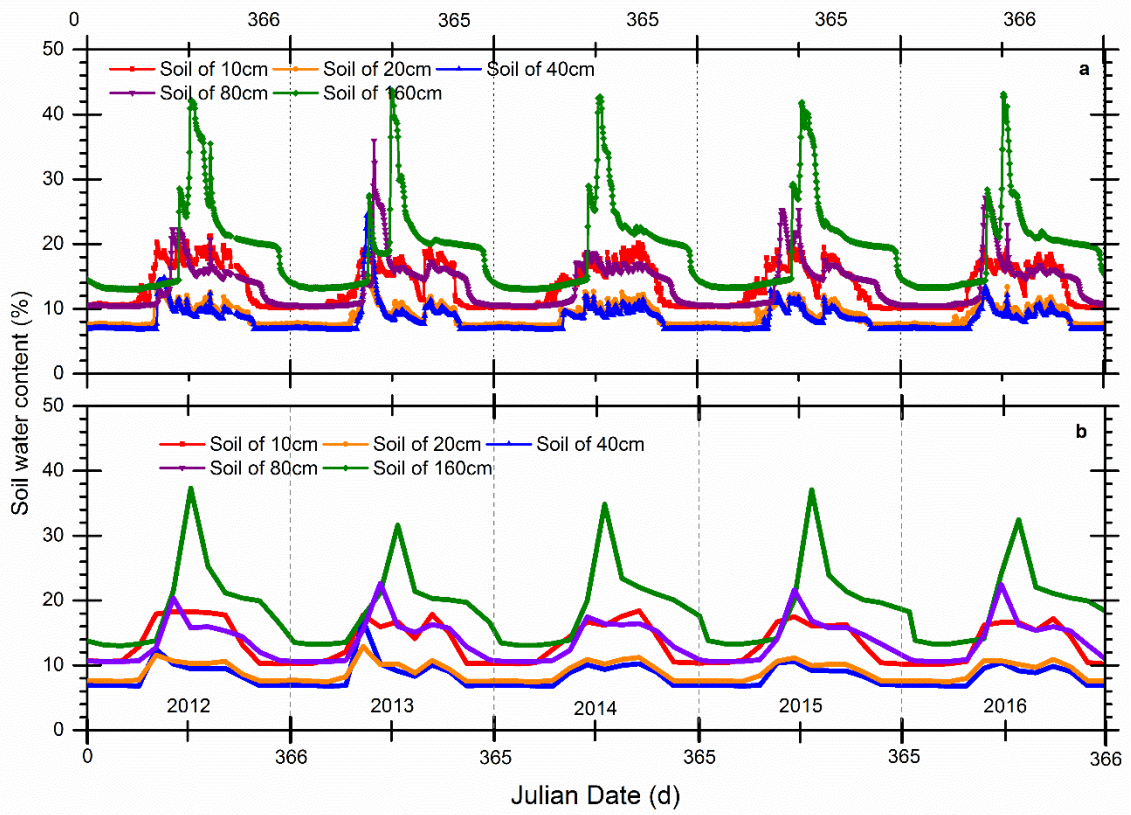

935

936 **Supplementary Figure 5.** Comparison between soil water content (SWC) of two different time

937 resolutions from 2012 to 2016, (a) is the half–hour scale SWC at soil depths of 10 cm, 20 cm, 40

938 cm, 80 cm, and 160 cm; and (b) is the 4–hour mean SWC for the same depths.

939

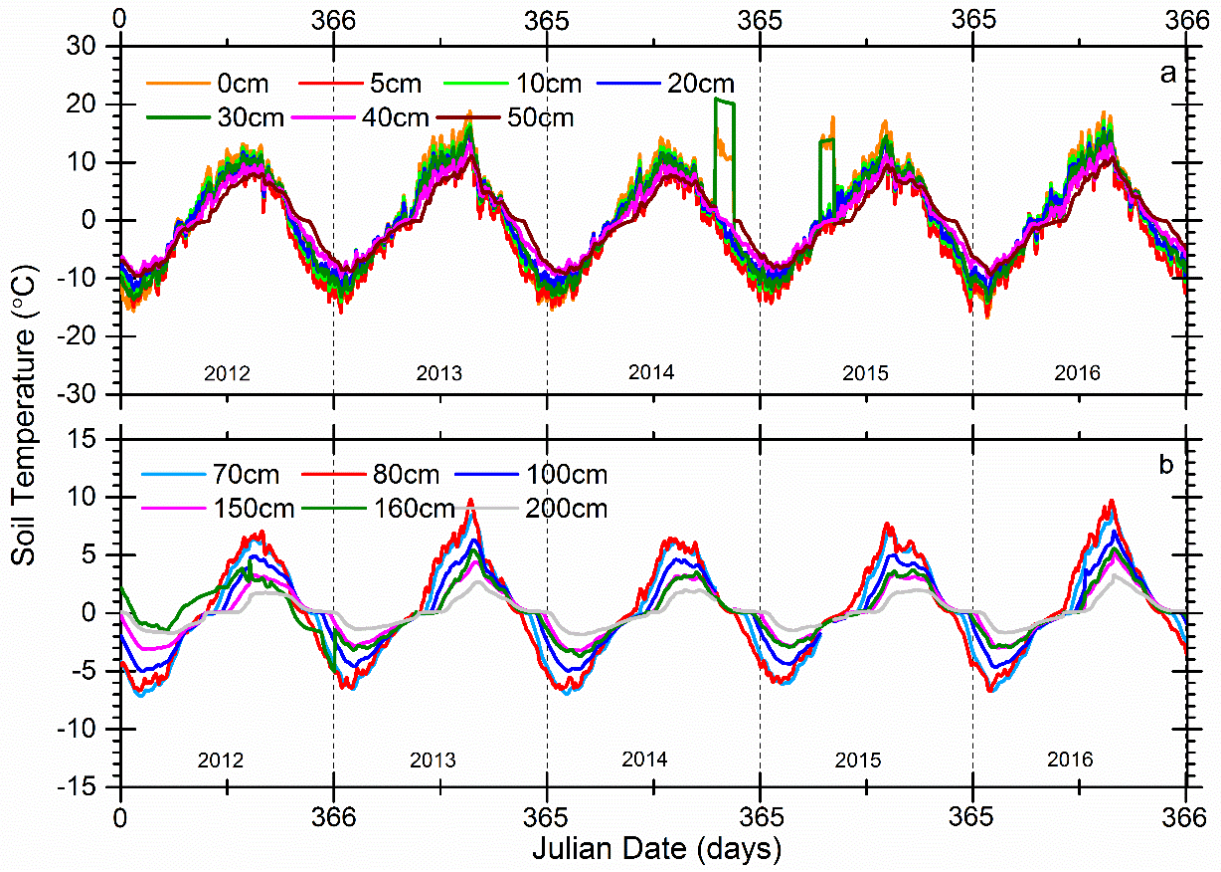

940

941 **Supplementary Figure 6.** Half–hour scale of 0 − 200 cm soil temperature (Tsoil) variations

942 from 2012 to 2016, (a) is for soil depths of 0 cm, 5 cm, 10 cm, 20 cm, 30 cm, 40 cm, 50 cm, (b)

943 is for soil depth of 70 cm, 80 cm, 100 cm, 150 cm, 160 cm, and 200 cm.

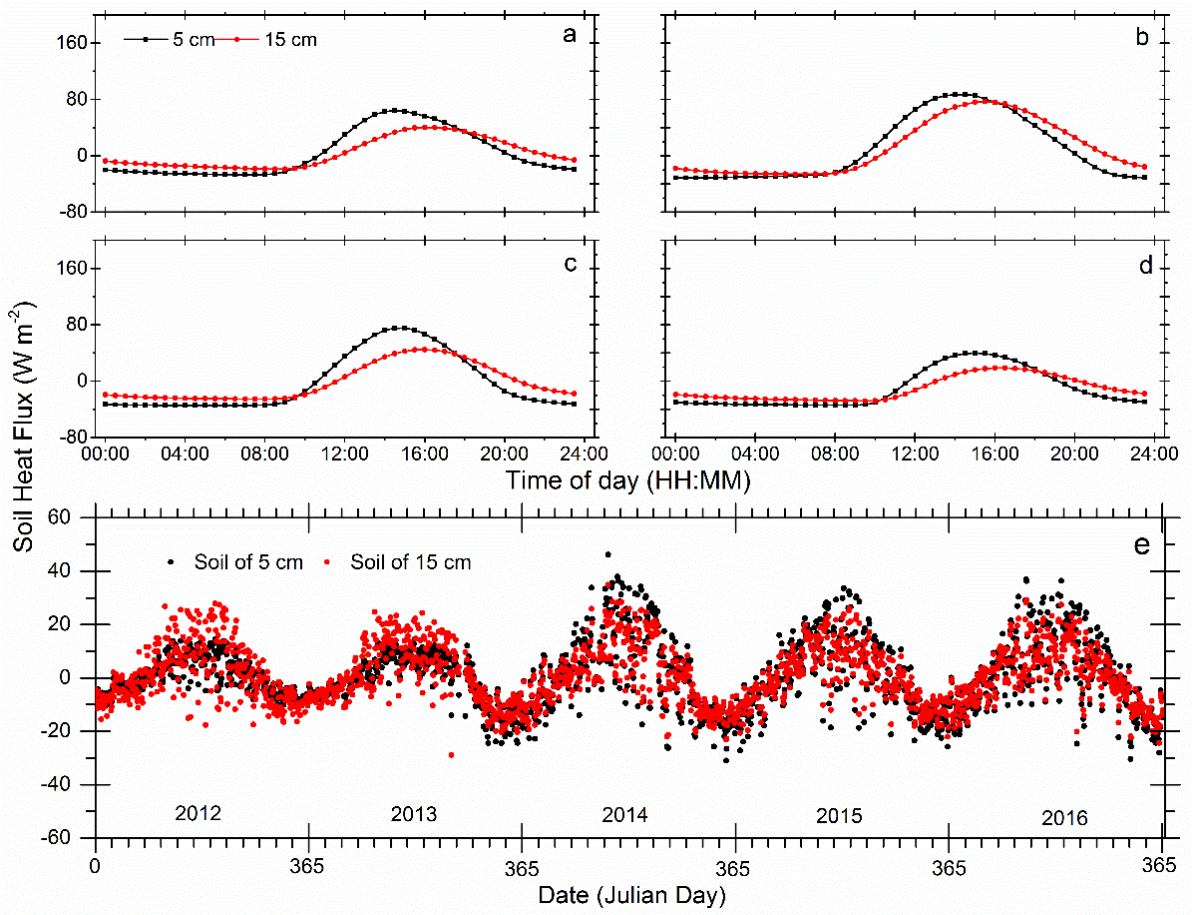

944

945 **Supplementary Figure 7.** Soil heat flux (SHF) at depth of 5 cm and 15 cm: (a), (b), (c), and (d)

946 are half–hour scale mean values in spring, summer, autumn, and winter, respectively; (e) shows

947 diel–scale mean values from 2012 to 2016.

948 .

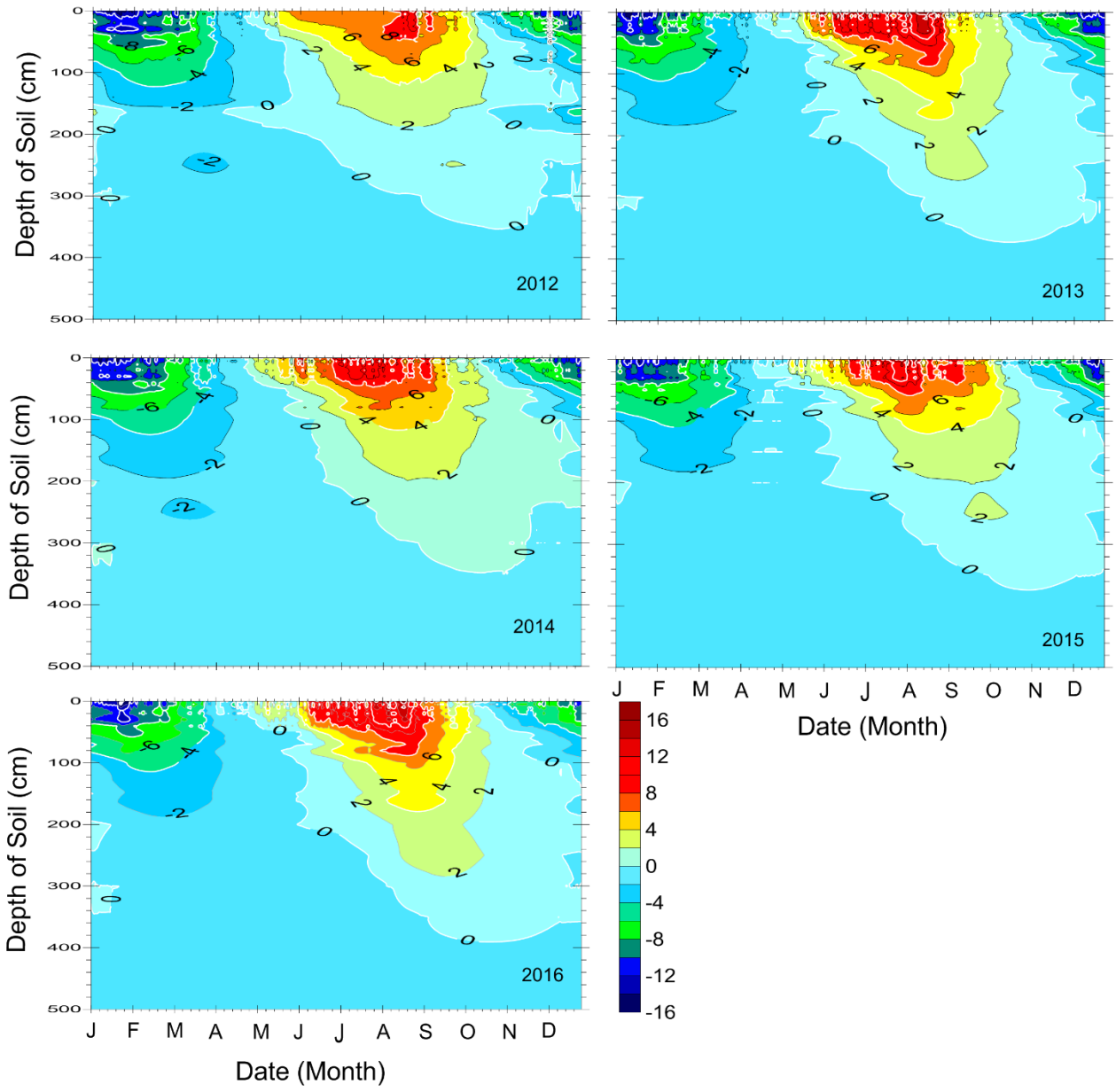

949

950 **Supplementary Figure 8.** Characteristics of the seasonal freezing and thawing processes of the

951 active layer for years: 2012, 2013, 2014, 2015, and 2016. Different colors represent the soil

952 temperature gradients from -16 °C to 20 °C. The depth of 0 °C represent the active layer

953 thickness (ALT).

954

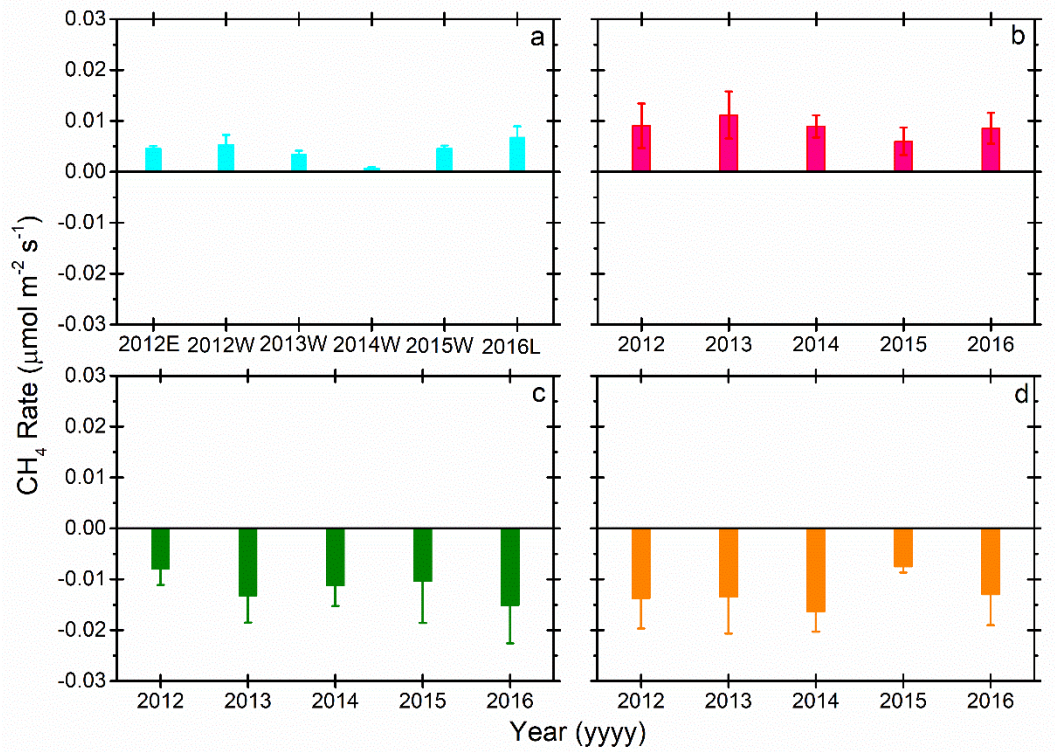

Supplementary Figure 9. Seasonal CH_4 rate mean value from 2012 to 2016: (a) is winter, (b) is spring, (c) is summer, and (d) is autumn. In the (a), 2012E is started from January 1st, 2012 and ended on February 17th, 2012; 2012W is started from 19th November, 2012 to 4th February, 2013; 2013W is started from 1st December, 2013 to 17th February, 2014; 2014W is started from 6th November, 2014 to 4th February, 2015; 2015W is started from 9th November, 2015 to 15th February, 2016; 2016L is started from October 26th, 2016 and ended on December 31st, 2016. All data are presented as mean values with standard deviations (mean ± standard deviation).

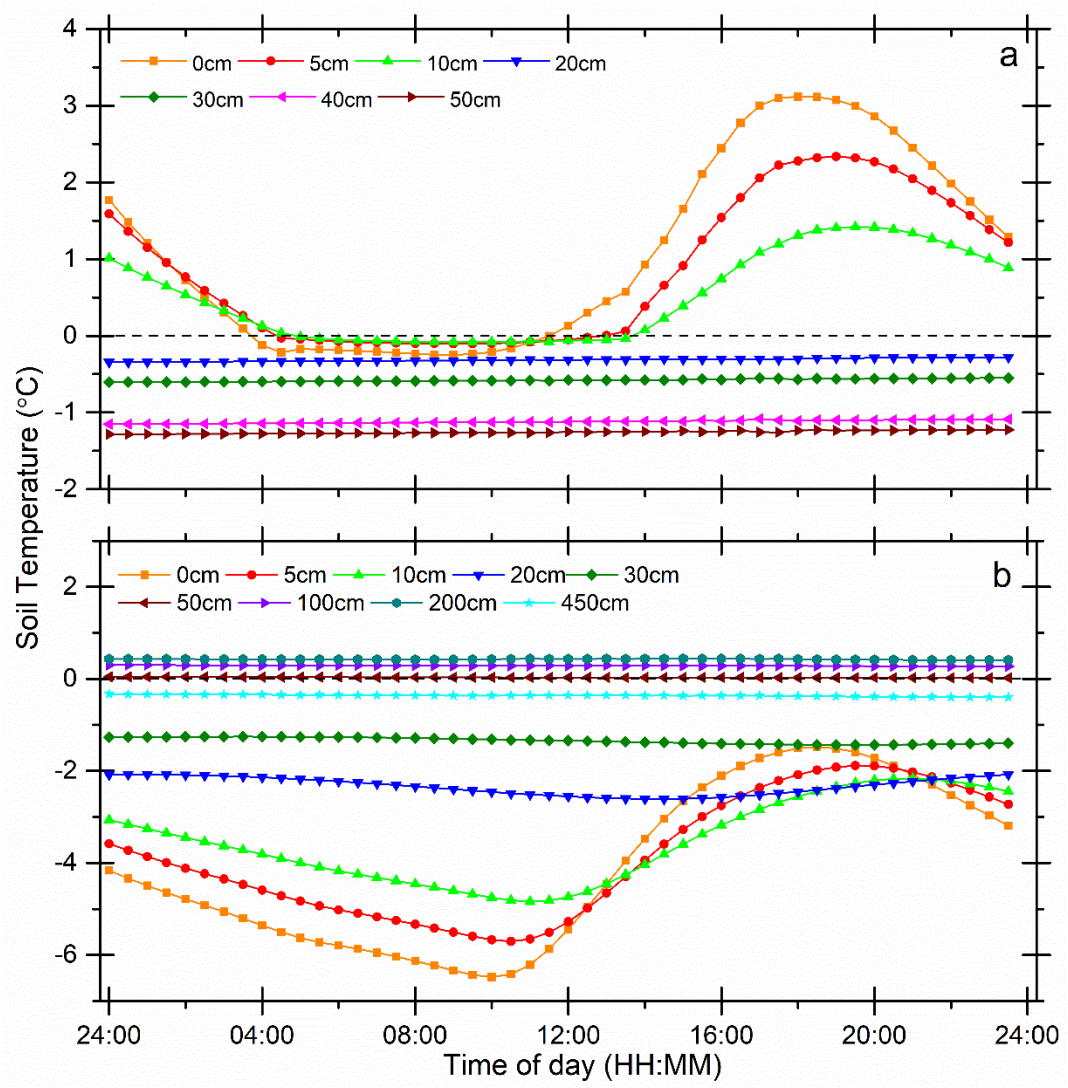

963

964 **Supplementary Figure 10.** Average half–hour scale of 0 − 450 cm soil temperature (Tsoil) diel
965 variations from 2012 to 2016, (a) is for spring_, (b) is for autumn_. Notedly, during spring, the
966 Tsoil of 100cm, 200cm, 450cm were all below -2 ℃ and during autumn_ the Tsoil of 40cm
967 almost overlap to Tsoil of 50cm, to make the figure more clearly, we removed the Tsoil of
968 100cm, 200cm, 450cm in figure (a) and removed the Tsoil of 40cm for figure (b).

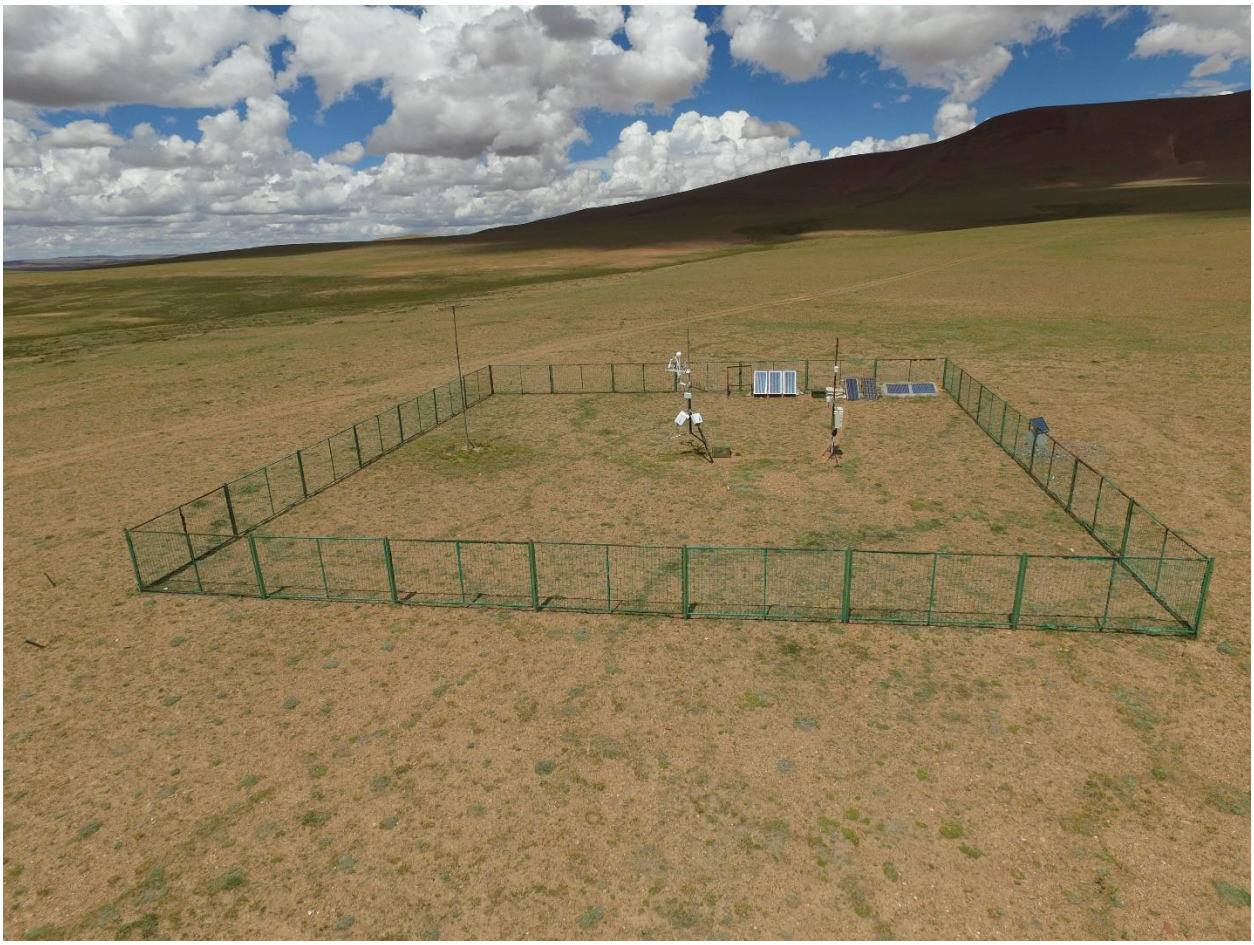

Supplementary Figure 11. A bird's eye view of the eddy covariance in Beilu'he station